The Abdus Salam
International Centre for Theoretical Physics

United Nations
Educational, Scientific and
Cultural Organization

IAEA
International Atomic Energy Agency

2048-2

From Core to Crust: Towards an Integrated Vision of Earth's Interior

20 - 24 July 2009

The Dynamics of compositional plumes

I. A. El Tayeb
Sultan Qaboos University, Muscat, Oman

THE DYNAMICS OF COMPOSITIONAL PLUMES

By
Ibrahim A. Eltayeb
Department of Mathematics and Statistics, College of Science, Sultan Qaboos University, P.O. Box 36, Postal Code 123, Muscat, Sultanate of Oman

---

From Core to Crust: Towards an Integrated Vision of Earth's Interior
Trieste, Italy, 20-24 July 2009

Contents

1. Introduction

Flow plumes play an important role in fluid mechanics with applications including different parts of the Earth, industry and the environment. In these note we will be concerned with compositional plumes. A compositional plume is here defined as uni-directional flow of a fluid in a column of finite thickness rising in another fluid of different composition and much larger length scale.

After briefly summerising the relevance of such plumes to different parts of the earth, we investigate the general properties of these plumes and we will not consider any detailed study of any one particular application. Also, we will restrict our analysis to plumes with sharp boundaries so that the material transported by the plume flow is compositionally very different from that of the surrounding fluid. This allows us to bring out the main properties of the dynamics more clearly.

The relevance of plumes to industry is mainly in metallurgical applications (Copley *et al.* 1970, Huppert 1990. Plumes are very important for studying the earth. Their first application to earth includes mantle convection (Morgan 1971, Loper and Stacey 1983, Ribe and Christensen 1994, White and McKenzie 19995, Steinberger 2000). Here they are believed to explain the flows between the plates (Zhao 2004) and also the powerful flows associated with hotspots and volcanic eruptions (Sleep 1990, Duncan 1991, Nolet *et al.* 2007) as well as in material transport (e.g. basalt) in the mantle (Hauri *et al.* 1994, Bonneville et al. 2006). The plume flows are also related to the reversals of the geomagnetic field (Loper and McCartney 1983, Larson and Olson 1991).

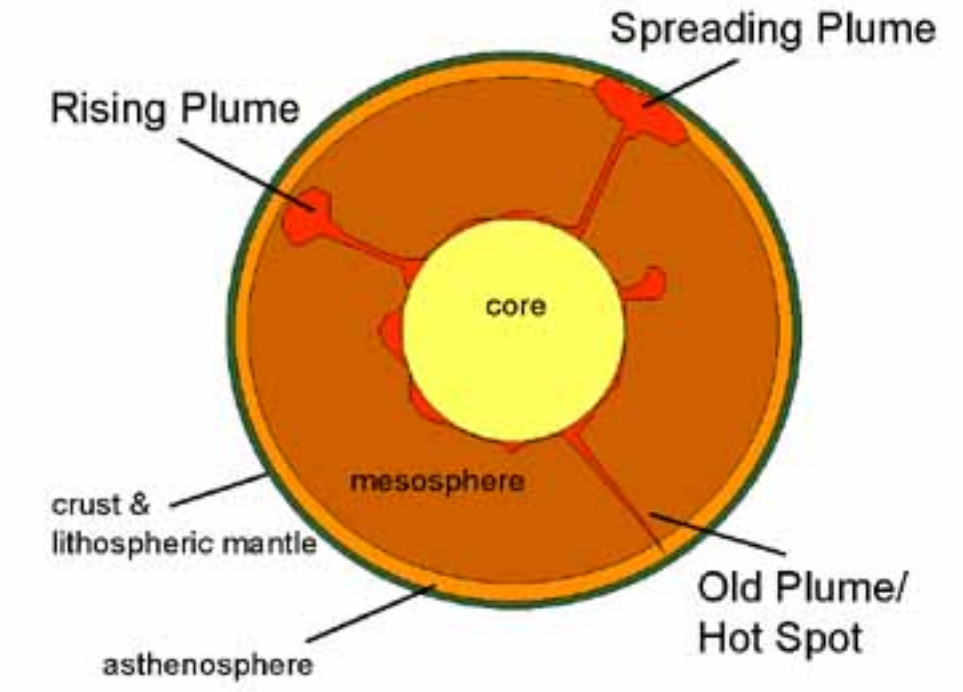

Figure 1. A schematic representation of Earth regions (with core standing for both fluid outer and solid inner cores) and hotspot types.

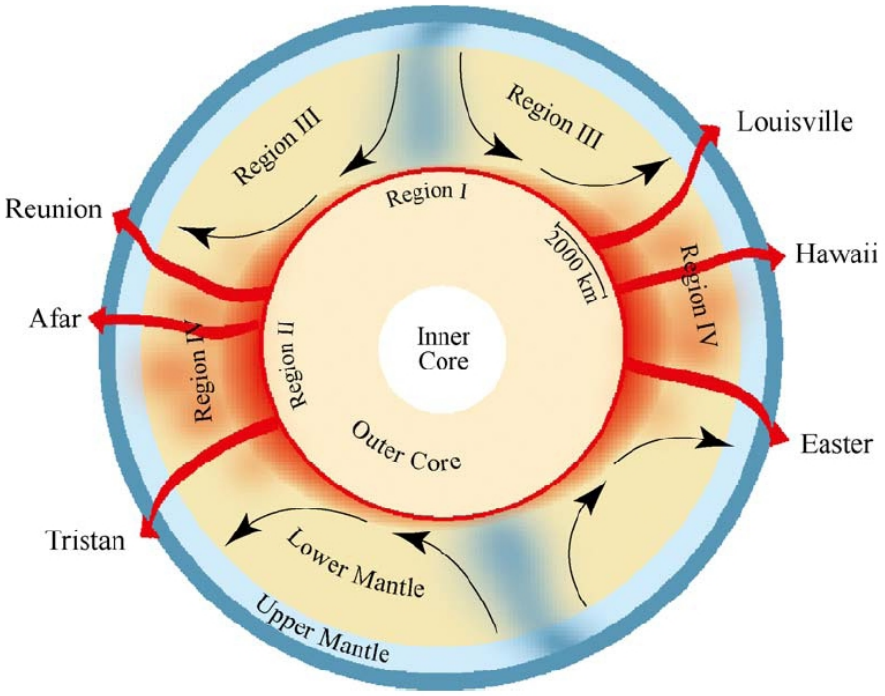

Figure 2. A schematic representation of mantle plumes and hotspots distribution

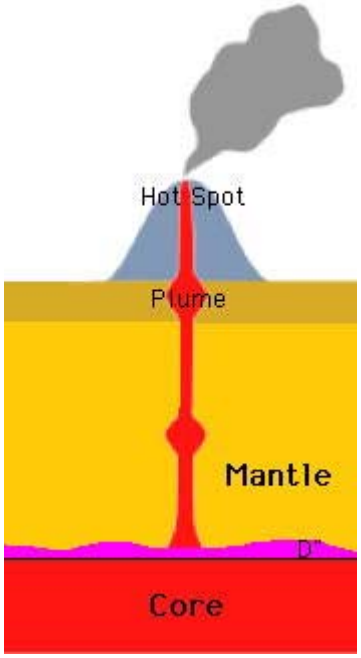

Figure 3. Schematic representation of a plume rising through the mantle to cause a volcanic eruption at an active hotspot.

In the late seventies, Loper and Roberts revived the suggestion first made by Verhoogen (1961) that the solidification of the outer core fluid to form the solid inner core released latent heat that contributed to the energy source for powering the geomagnetic field of the earth. Loper and Roberts (1978) and Roberts and Loper (1978) developed a theory for the solidification process at the inner-outer core boundary. Although the temperature at the inner core surface is much higher than at the top of the outer core, the solidification takes place at the inner core boundary due to the increased pressure with depth. The fluid outer core is an alloy composed mainly of the heavy component of molten iron and lighter elements which are believed to include sulphur, oxygen, nitrogen, hydrogen etc. The heavy iron component of the outer core fluid alloy solidifies first thus forming a thin layer on the surface of the inner core of mixed solid crystals (mainly of iron) and fluid other components. This layer of mixture of solid and fluid is called a mushy layer. Such a layer has been investigated in detail by Hills *et al*. (1983) in a fundamental paper on this subject.
The solidification process releases latent heat giving rise to a heat flux out of the layer and into the fluid core. Such release of energy has implications on fluid motions in the core and the regeneration of the geomagnetic field by dynamo action (Loper 1978, Loper and Roberts 1979, 1981).

The mushy layer has been studied recently by many researchers because of its relevance to Earth and industry. The reader is directed to reviews for further references (Loper 1987, Worster 1997).

The process of solidification continues with time and it has been shown that when such a layer increases to a certain level the top-heavy situation created by the solidification of the heavy component (so the mushy layer has lighter fluid compared to the overlying alloy), it becomes unstable (Worster 1992). The instability of the mushy layer takes the form of thin filaments of light fluid rising through the outer core fluid. These filaments are compositional plumes transporting the light fluid components from the mushy layer through the outer fluid core alloy. The instability of the plumes rising into the outer core may result in the break-up of these plumes into blobs that stir the outer fluid core producing small-scale motions which may produce helicity and $\alpha-$effect thus contributing to the geodynamo (Moffatt 1989, Moffatt and Loper, 1994).

It is then clear that there is considerable geophysical interest in compositional plumes. This indicates a need to understand the basic properties of compositional plumes. Rather than study a particular situation with a particular application, we will embark on studying the basic dynamical properties of compositional plumes. The effects of magnetic fields and rotation acting separately or together on the plume will also be examined.

The process of the formation of the mushy layer and the instabilities associated with it are illustrated using the famous aqueous ammonium Chloride (NH_4+H_2O) solution, first used by Copley *et. al*. (1970) and later by Huppert (1990) and others. When such

a solution prepared at 50 ^{0}C with a concentration of 28% by weight and placed on a ice-cold surface, the mushy layer can be seen to develop and when it is thick enough, instability appears and plumes rise into the melt. The plumes themselves are sometimes seen to disintegrate. Such a process may also be considered a form of instability. This provided the motivation for the study of the stability of these compositional plumes under laboratory and geophysical conditions (Eltayeb and Loper, 1991,1994, 1997, Eltayeb and Hamza 1998, Classen et al. 1999, Eltayeb 1999, Eltayeb et. al. 2004,2005, Eltayeb 2006).

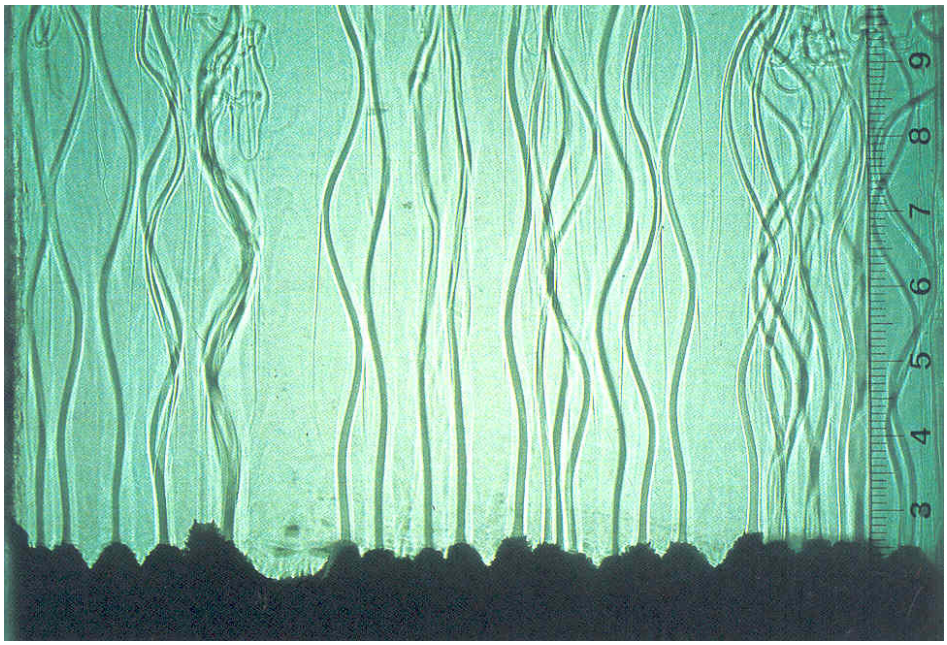

Figure 4. Aqueous ammonium chloride solution (Huppert, 1990).

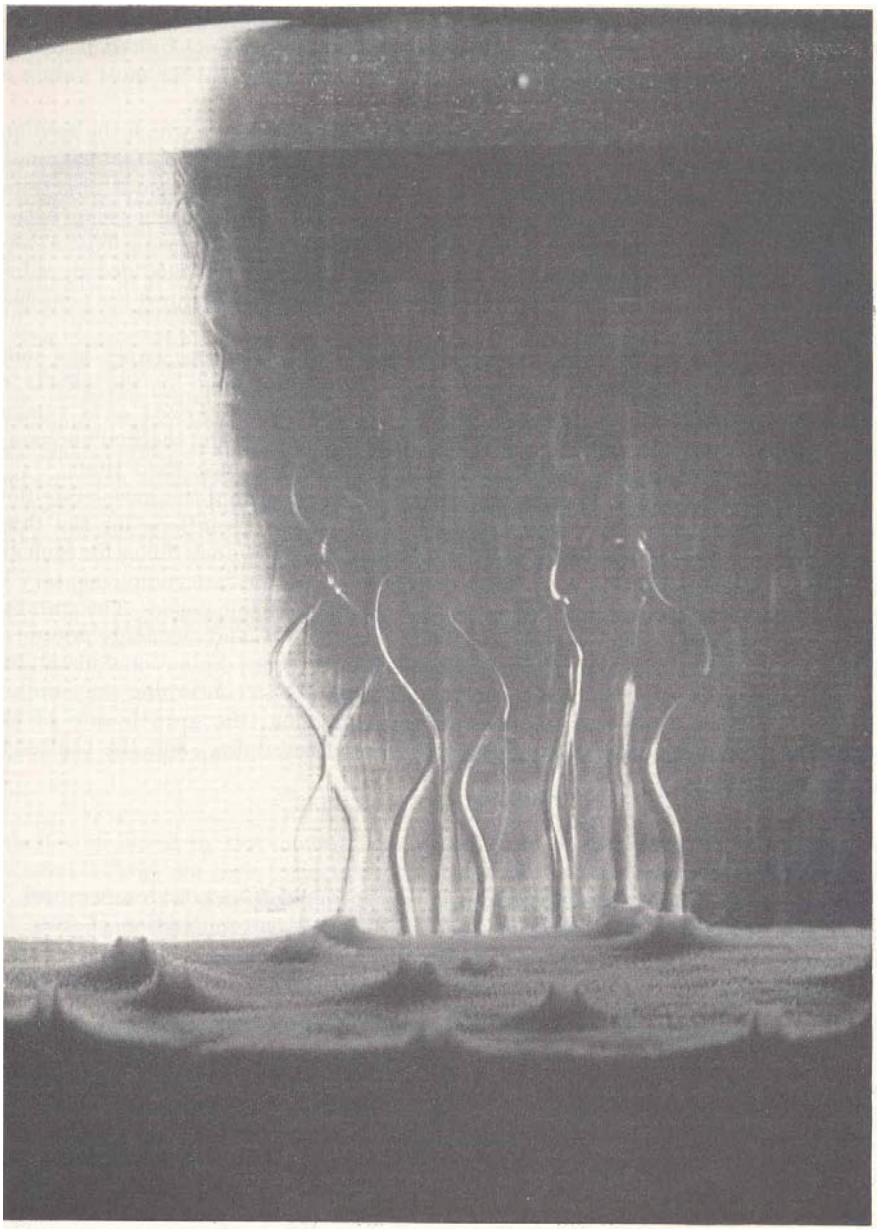

Figure 5. Aqueous ammonium Chloride solution (Eltayeb and Loper, 1991).

2.Formulation

Consider a column of light material of thickness $2\tilde{x}$ rising in a two-component, electrically conducting and less buoyant fluid of infinite extent. Both fluids possess the same kinematic viscosity, ν, thermal diffusivity, κ, magnetic diffusivity, η. The material diffusion is negligible. The equation of state of the system has the form

$$\tilde{\rho} / \tilde{\rho}_0 = 1 - \alpha(\tilde{T} - \tilde{T}_0) - \beta(\tilde{C} - \tilde{C}_0) \qquad (2.1)$$

in which $\tilde{\rho}$ is the density, $\tilde{T}$ is the temperature, $\tilde{C}$ is the concentration of light material, α is the coefficient of thermal expansion, β the coefficient of compositional expansion and a subscript denotes a reference value. The other

equations of the system are, respectively, those of linear momentum, heat, induction, material diffusion, continuity and Gauss' law:

$$\tilde{\rho}_0\left[\partial\tilde{\mathbf{u}}/\partial\tilde{t}+\left(\tilde{\mathbf{u}}\cdot\nabla\right)\tilde{\mathbf{u}}+2\boldsymbol{\omega}\times\tilde{\mathbf{u}}\right]=-\nabla\tilde{p}+\tilde{\rho}_0\nu\nabla^2\tilde{\mathbf{u}}+\mu^{-1}\nabla\times\tilde{\mathbf{B}}\times\tilde{\mathbf{B}}-\tilde{\rho}g\,\hat{\mathbf{z}} \quad (2.2)$$

$$\partial\tilde{T}/\partial\tilde{t}+\tilde{\mathbf{u}}\cdot\nabla\tilde{T}=\kappa\nabla^2\tilde{T} \quad (2.3)$$

$$\partial\tilde{\mathbf{B}}/\partial\tilde{t}=\nabla\times(\tilde{\mathbf{u}}\times\tilde{\mathbf{B}})+\eta\nabla\tilde{\mathbf{B}} \quad (2.4)$$

$$\partial\tilde{C}/\partial\tilde{t}+\tilde{\mathbf{u}}\cdot\nabla\tilde{C}=0 \quad (2.5)$$

$$\nabla\cdot\tilde{\mathbf{u}}=0,\quad \nabla\cdot\tilde{\mathbf{B}}=0 \quad (2.6)$$

Here $\tilde{\mathbf{u}}$ is the velocity, $\tilde{p}$ the pressure, $\tilde{\mathbf{B}}$ the magnetic induction, $\tilde{T}$ the temperature, $\tilde{t}$ the time, $\boldsymbol{\omega}$ the angular velocity, μ the magnetic permeability, g the uniform gravitational acceleration and $\hat{\mathbf{z}}$ is a unit vector in the direction opposite to that of the gravity. Note here that we have used a tilde to refer to dimensional variables.

We intend to investigate a solution of these equations in the form of a uni-directional flow rising vertically (i.e. in a direction opposite to that of gravity) in a column of finite thickness surrounded by in infinite fluid having the same material properties. The first step is to cast the equations into dimensionless form. To do this, we note that the system (2.2)-(2.6) allows a static solution in which the flow, temperature and magnetic induction are

$$\tilde{\mathbf{u}}=\mathbf{0},\ \ \tilde{\mathbf{B}}=\mathbf{B_0},\ \ \tilde{T}=\gamma\tilde{z}+\tilde{T}_0,\ \ \tilde{C}=\tilde{C}_0 \quad (2.7)$$

where $\tilde{z}$ is the coordinate measured vertically upwards, $\mathbf{B}_0$ is a constant and the pressure is governed by

$$\nabla\tilde{p}=-g\hat{\mathbf{z}}\tilde{\rho}_o\left[1-\alpha\gamma\tilde{z}\right] \quad (2.8)$$

This solution can be used to identify the characteristic units of the relevant variables. It transpires that the appropriate length scale for the problem is the salt finger length scale defined by

$$L=\left(\nu\kappa/\alpha\gamma g\right)^{1/4} \quad (2.9)$$

We take the difference between the concentrations of the column and surrounding fluid, $\tilde{C}_d$, as the characteristic unit of concentration of light material. Our interest lies in motions due to this difference in concentration and for this reason we take a unit of velocity, U, as

$$U=\beta\tilde{C}_d\left(g\kappa/\alpha\gamma\nu\right)^{1/2} \quad (2.10)$$

and in order to maintain a balance between compositional buoyancy and temperature stratification, we take $\beta\tilde{C}/\alpha$ as a unit of temperature. Finally, the unit of pressure is taken as $\tilde{\rho}_0\beta\tilde{C}_d\left(g^3\nu\kappa/\alpha\gamma\right)^{1/4}$ and that of magnetic induction is $\left|\mathbf{B_0}\right|$. The appropriate time scale for the instabilities is the convective time scale

$$t_c=L/U=\nu/\beta\tilde{C}gL \quad (2.11)$$

The dimensionless equations can now be written as:

$$R\frac{D\mathbf{u}}{Dt}+\tau\boldsymbol{\omega}\times\mathbf{u}=-\nabla p+\nabla^2\mathbf{u}+\frac{Qc}{\sigma_m R}\left(\mathbf{B}\cdot\nabla\right)\mathbf{B}+\left(C-C_0+T-T_0-\frac{1}{\beta\tilde{C}}\right)\hat{\mathbf{z}} \quad (2.12)$$

$$\sigma RDT/Dt+\mathbf{u}\cdot\hat{\mathbf{z}}=\nabla^2T \quad (2.13)$$

$$\sigma_m R\,\partial\mathbf{B}/\partial t=\sigma_m R\nabla\times(\mathbf{u}\times\mathbf{B})+\nabla\mathbf{B} \quad (2.14)$$

$$DC/Dt=0 \quad (2.15)$$

$$\nabla \cdot \mathbf{u} = 0, \quad \nabla \cdot \mathbf{B} = 0 \tag{2.16}$$

Here the variables without a tilde are dimensionless and we used the mobile operator

$$\frac{D}{Dt} \equiv \frac{\partial}{\partial t} + \mathbf{u}.\nabla \tag{2.17}$$

The equations (2.12)-(2.16) involve five dimensionless numbers : the Prandtl number, σ, the magnetic Prandtl number, σ_m, R (measure of compositional buoyancy), the Taylor number, *Ta* (which is a measure of rotation), and the Chandrasekhar number, *Qc* (which is a measure of the magnetic filed). They are defined by

$$\sigma = \frac{\nu}{\kappa}, \quad \sigma_m = \frac{\nu}{\eta}, \quad R = \frac{UL}{\nu}, \quad Ta = \left(\frac{2|\boldsymbol{\omega}|L^2}{\nu} \right)^2 = \tau^2, \quad Qc = \frac{|\mathbf{B_0}|^2 L^2}{\mu \rho \nu \eta}, \tag{2.18}$$

As we are interested in plume flows, we assume solutions of the form

$$\mathbf{u}(x, y, z, t) = \mathbf{0} + \bar{w}(x)\hat{\mathbf{z}} + \varepsilon \mathbf{u}^{\dagger}(x, y, z, t) \tag{2.19}$$

$$p(x, y, z, t) = p_b + \bar{p}(x) + \varepsilon p^{\dagger}(x, y, z, t) \tag{2.20}$$

$$T(x, y, z, t) = T_b + \bar{T}(x) + \varepsilon T^{\dagger}(x, y, z, t) \tag{2.21}$$

$$\mathbf{B}(x, y, z, t) = \mathbf{B}_0 + \sigma_m Re \varepsilon \mathbf{b}^{\dagger}(x, y, z, t) \tag{2.22}$$

$$C(x, y, z, t) = C_0 + \bar{C}(x) + \varepsilon C^{\dagger}(x, y, z, t) \tag{2.23}$$

where

$$p_b = p_0 - \frac{(z - z_0)}{\beta \tilde{C}} + \frac{(z - z_0)^2}{2\sigma R} + \frac{Qc\,|\mathbf{B}|^2}{2\sigma_m R}, \qquad T_b = T_0 + \frac{(z - z_0)}{\sigma R} \tag{2.24}$$

The variables with subscript 'b' refer to the state (2.7) while the variables with an 'overbar' constitute a mean state driven by thermal and viscous diffusions and those with a dagger superscript correspond to perturbations of small amplitude ε.

The unit vectors along the magnetic field and rotation are assumed of the form

$$\hat{\boldsymbol{\omega}} = (0, \omega_H, \omega_z), \quad \hat{\mathbf{B}}_0 = (0, B_H, B_z) \tag{2.25}$$

in which

$$\omega_H^2 + \omega_z^2 = 1, \qquad B_H^2 + B_z^2 = 1 \tag{2.26}$$

Note that both rotation vector and magnetic induction have no components in the $x-$direction. This is because non-zero components for a basic state depending on x only is associated with difficulties that complicate the situation and we will not dwell on them here.

We now substitute from equations (2.19)-(2.23) into equations (2.12)-(2.16) to obtain equations involving both mean state variable and fluctuating variables. If we neglect all terms proportional to ε^2 or smaller, and take the mean of the equations we obtain the mean state equations as

$$\frac{d\bar{p}}{dx} = -\omega_H \tau \bar{w}(x) \tag{2.27}$$

$$\frac{d^2\bar{w}}{dx^2} - \bar{T} = \bar{C} \tag{2.28}$$

$$\frac{d^2\bar{T}}{dx^2} - \bar{w} = 0 \tag{2.29}$$

Equations (2.28) and (2.29) can be combined in

$$\frac{d^2Y}{dx^2} - iY = i\bar{C}, \qquad Y = \bar{T} - i\bar{w} \tag{2.30}$$

The basic state equation for $\bar{C}$ is automatically satisfied (because the material diffusion has been neglected). It is then left to us to choose the form of $\bar{C}$. We will deal with this later.

If we subtract equations (2.27)-(2.29) from equations (2.12)-(2.16) after using (2.19)-(2.24) and neglecting terms proportional to ε^2, we obtain the linearised perturbation equations of the problem as

$$\nabla^2\mathbf{u}^\dagger + Qc\left(\hat{\mathbf{B}}_0\cdot\nabla\right)\mathbf{b}^\dagger + \left(C^\dagger + T^\dagger\right)\hat{\mathbf{z}} - \nabla p^\dagger - \tau\hat{\boldsymbol{\omega}}\times\mathbf{u}^\dagger = R\left[\frac{\partial\mathbf{u}^\dagger}{\partial t} + \bar{w}\frac{\partial\mathbf{u}^\dagger}{\partial z} + \left(\mathbf{u}^\dagger\cdot\hat{\mathbf{x}}\right)D\bar{w}\,\hat{\mathbf{z}}\right] \tag{2.31}$$

$$\nabla^2 T^\dagger - \mathbf{u}^\dagger\cdot\hat{\mathbf{z}} = \sigma R\left[\frac{\partial T^\dagger}{\partial t} + \bar{w}\frac{\partial T^\dagger}{\partial z} + \left(\mathbf{u}^\dagger\cdot\hat{\mathbf{x}}\right)D\bar{T}\right] \tag{2.32}$$

$$\nabla^2\mathbf{b}^\dagger + \left(\hat{\mathbf{B}}_0.\nabla\right)\mathbf{u}^\dagger = \sigma_m R\left[\frac{\partial\mathbf{b}^\dagger}{\partial t} - D\bar{w}\left(\hat{\mathbf{x}}\cdot\mathbf{b}^\dagger\right)\hat{\mathbf{z}}\right] \tag{2.33}$$

$$\frac{\partial C^\dagger}{\partial t} + \bar{w}\frac{\partial C^\dagger}{\partial z} = 0 \tag{2.34}$$

$$\nabla\cdot\mathbf{u}^\dagger = 0, \quad \nabla\cdot\mathbf{b}^\dagger = 0 \tag{2.35}$$

We are now required to solve the equations (2.27)-(2.30) for the basic state after the form of $\bar{C}$ has been prescribed and then examine the stability of the basic state solution using equations (2.31)-(2.35) together with the appropriate boundary conditions.

A good understanding of the dynamics of plumes is perhaps acquired by first studying an idealised model and then improving it gradually. This will help us to understand the dynamical significance of the various factors affecting the dynamics of the plumes.

3. The Cartesian plume

Consider a Cartesian system of coordinates $O(x, y, z)$ in which Oz is vertically upwards and Ox, Oy are horizontal. Assume a top-hat profile for the basic state concentration of light material.

$$\bar{C} - C_0 = \begin{cases} 1 & \text{if } |x| < x_0 \\ 0 & \text{if } |x| > x_0 \end{cases} \tag{3.1}$$

This represents a column of light material, of dimensionless thickness $2x_0$, rising in an infinite less buoyant fluid (see Figure 6). This model is called the "Cartesian Plume" for convenience.

The column is bounded by two vertical interfaces at $x = \pm x_0$ across which the concentration of light material C experiences sudden jumps. This is not a very realistic form of basic concentration profile but it is a very good approximation to plume carrying material of a very different nature from its surroundings. The two

vertical interfaces remain material surfaces and the boundary conditions at every interface are:

(i) continuity of velocity
(ii) continuity of magnetic field
(iii) continuity of linear momentum
(iv) continuity of temperature
(v) continuity of heat flux
(vi) continuity of magnetic flux
(vii) the interface is a material surface

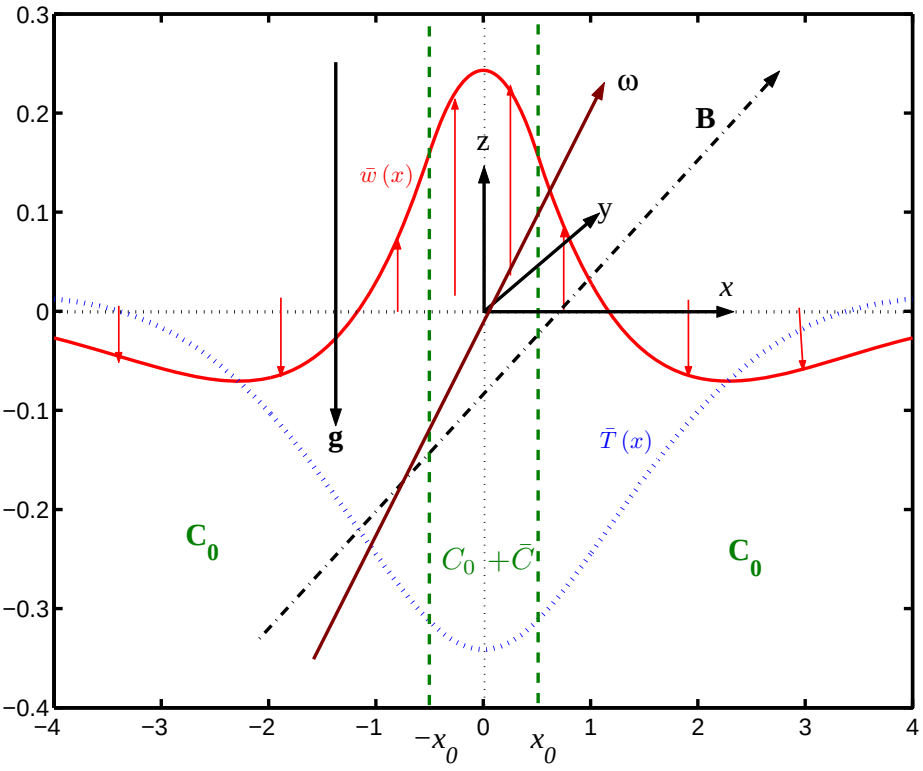

Figure 6. The geometry of the model. The plume is contained between the two discontinuous vertical lines at $x = \pm x_0$, shown here for $x_0 = 0.5$.

3.1 The basic state of the Cartesian plume

The basic state equations (2.30) and (2.27) can easily be solved subject to the conditions that Y , dY/dx , to get

$$Y(x) = \begin{cases} e^{-kx_0}\cosh(kx) - 1, & |x| < x_0 \\ -\exp(-k|x|)\sinh(kx_0), & |x| > x_0 \end{cases}, \qquad (3.2)$$

and

$$\frac{\bar{p}(x)}{\omega_H \tau} = \mathrm{Im}\begin{cases} e^{-kx_0}\sin(kx)/k, & |x| < x_0 \\ \mp\exp(-k|x|)\sinh(kx_0)/k, & |x| > x_0 \end{cases} \qquad (3.3)$$

where

$$k = (1+i)/\sqrt{2} \tag{3.4}$$

The solution (3.2) and (3.3) is illustrated in Figure 7. We see that the pressure which is non-zero only when the rotation vector is inclined to the vertical is an odd function of x while the flow and temperature are both even in x .

The flow is oscillatory and this has an effect on the flow within the plume. If the plume is wide, the flow within the plume can slow down in the middle of the plume or even reverse direction. This has the effect on the material transport which can decrease for certain thicknesses of the plume.

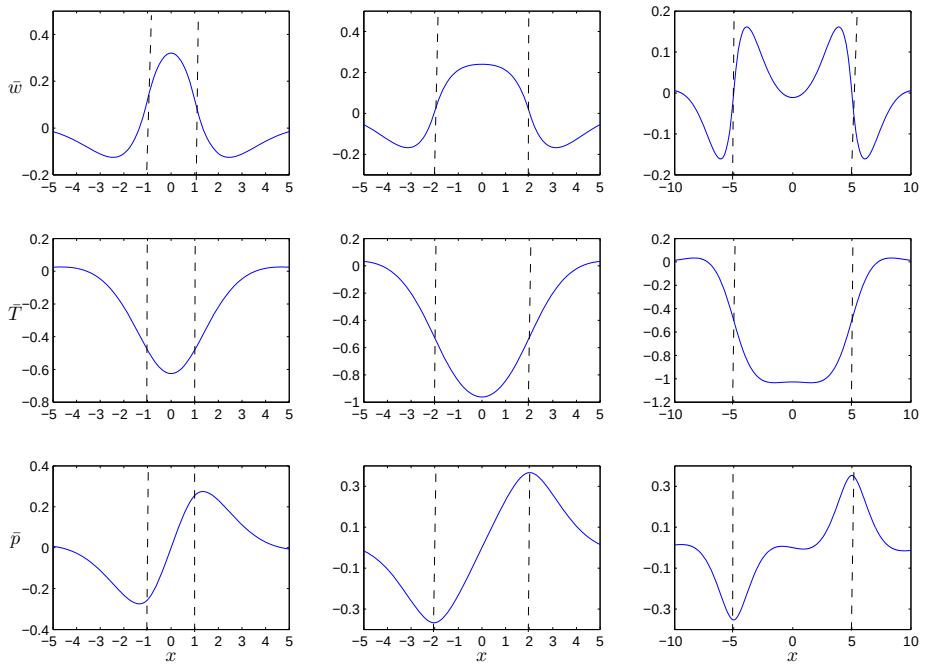

Figure 7. The profiles of the basic state of the Cartesian plume variables $\bar{w}, \bar{T}, \bar{p}$ for 3 different plume thickness. Note the reverse flow when $x_0 = 5.0$

The basic state (3.2) is associated with material, heat and buoyancy fluxes governing the transport of light material upwards and heat downwards resulting in a total flux, $\tilde{F}_B$. These fluxes are defined by

$$\tilde{F}_m = \frac{1}{2L}\int_{-\infty}^{\infty} \tilde{w}\left(\tilde{C} - \tilde{C}_0\right)dA, \quad \tilde{F}_H = \frac{1}{2L}\int_{-\infty}^{\infty} \tilde{w}\left(\tilde{T} - \tilde{T}_0\right)dA, \quad \tilde{F}_B = \alpha\tilde{F}_H + \beta\tilde{F}_m \tag{3.5}$$

where the integrals are taken over a specified area and L is a measure of the horizontal length of the interfaces. We use the characteristic units of $\beta^2\tilde{C}_d^2\left(g\kappa^3/\nu\alpha^3\gamma^3\right)^{1/4}$, $\beta\tilde{C}_d^2\left(g\alpha\kappa^3/\nu\gamma^3\right)^{1/4}$, $\beta^2\tilde{C}_d^2\left(g\alpha\kappa^3/\nu\alpha^3\gamma^3\right)^{1/4}$ of heat, respectively, material and buoyancy fluxes to get the expressions

$$F_m = \frac{1}{2}\int_{-\infty}^{\infty} \bar{w}\bar{C}dx, \quad F_H = \frac{1}{2}\int_{-\infty}^{\infty} \bar{w}\bar{T}dx, \quad F_B = F_m + F_H \tag{3.6}$$

Using the expressions (3.2) and (3.1) in (3.6) we obtain

$$F_m = \frac{\sqrt{2}}{4}\left\{1-e^{-x_0\sqrt{2}}\left[\cos\left(x_0\sqrt{2}\right)+\sin\left(x_0\sqrt{2}\right)\right]\right\} \tag{3.7}$$

$$F_H = \frac{1}{4}x_0 e^{-x_0\sqrt{2}}\sin\left(x_0\sqrt{2}\right)+\frac{3\sqrt{2}}{16}\left\{-1+e^{-x_0\sqrt{2}}\left[\cos\left(x_0\sqrt{2}\right)+\sin\left(x_0\sqrt{2}\right)\right]\right\} \tag{3.8}$$

$$F_B = \frac{1}{4}x_0 e^{-x_0\sqrt{2}}\sin\left(x_0\sqrt{2}\right)+\frac{\sqrt{2}}{16}\left\{1-e^{-x_0\sqrt{2}}\left[\cos\left(x_0\sqrt{2}\right)+\sin\left(x_0\sqrt{2}\right)\right]\right\} \tag{3.9}$$

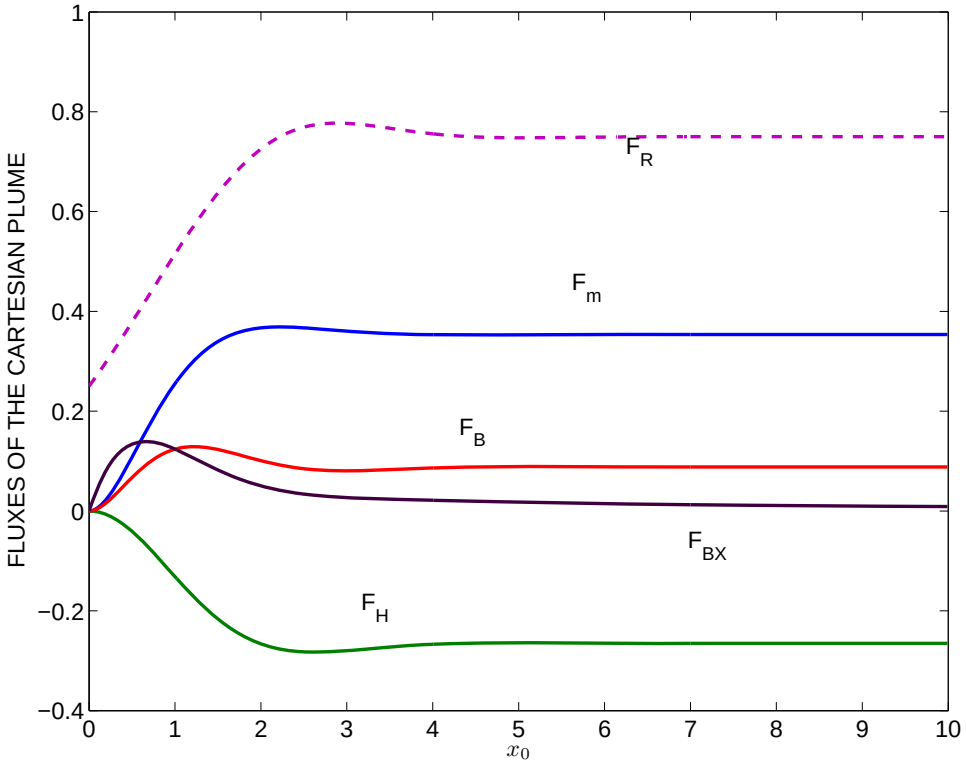

Figure 8. The profiles of the fluxes of the basic state of the Cartesian plume.

The dependence of these fluxes on the thickness of the plume is illustrated in Figure 8. We find that the material diffusion increases from 0 at $x_0 = 0$ to a maximum value of 0.36883 at x_0= 2.21102 and then decreases to a local minimum of 0.35291 at x_0=4.44103 and increases again to 0.35358 at x_0= 6.72 before it decreases slowly to a limiting value of $\sqrt{2}/4$ as $x_0 \to \infty$. The negative heat flux decreases from 0 at $x_0 = 0$ to a minimum of -0.28277 at x_0= 2.632 before it increases to a maximum of -0.26408 at x_0= 4.913 and then decreases gradually to $-3\sqrt{2}/16$ as $x_0 \to \infty$. The total buoyancy, F_B, which is the sum of the material and heat fluxes also oscillates as x_0 increases. It increases from 0 to a maximum of 0.12893 at x_0= 1.221 and then decreases to 0.08048 at x_0= 2.99

before it increases to a local maximum of 0.08905 at $x_0 =$ 5.116 and then decreases to a local minimum of 0.08835 at $x_0 =$7.35 before it increases slowly to a limiting value of $\sqrt{2}/16$ as $x_0 \to \infty$. The ratio, $F_r = \left| F_H / F_m \right|$ behaves in a way similar to the buoyancy flux; it acquires two local maxima of 0.77718, 0.75103 at x_0 = 2.886, 7.264, respective, separated by a local minimum of 0.74786 at $x_0 =$ 5.052 and approaches the value 0.74999 as $x_0 \to \infty$. This shows that the material flux always exceeds the numerical value of the heat flux resulting in a positive buoyancy flux for all $x_0 \neq 0$. This result will have a profound result on the stability of the plume flow, as we shall see later. It is interesting to note that the normalised buoyancy flux, F_{BX}, also vanishes for $x_0 = 0$ and increases to a maximum of 0.13926 at $x_0 = 0.66$ before it decays to 0 as $x_0 \to \infty$.

3.2 The stability of the Cartesian plume

It is of interest to examine the stability of the plume flow obtained above. The stability problem has been discussed in detail by Eltayeb and Loper (1994). Here we will give the main points of the analysis.

Eltayeb and Loper found that instability sets in for all non-zero values of the forcing parameter R. They then adopted an expansion in the small parameter R in order to examine the linear stability of the plume.
The stability of the system is examined by assuming that the surface at $x = x_0$ is given a small harmonic disturbance of the form

$$x = x_0 + \varepsilon \exp\left[\Omega t + i\left(my - nz\right)\right] + c.c, \tag{3.10}$$

in which c.c. stands for the 'complex conjugate'. Here Ω is the growth rate and (m,n) are the wavenumber components in the y,z plane. The disturbance (3.10) will propagate into the infinite fluid so that

$$\begin{aligned}&\left\{\mathbf{u}^{\dagger}, p^{\dagger}, T^{\dagger}, C^{\dagger}\right\}\\ &\quad = \left\{\mathbf{u}(x), -inp(x), T(x), C(x)\right\}\exp\left[\Omega t + i\left(my - nz\right)\right] + c.c\end{aligned} \tag{3.11}$$

and the interface at $x = -x_0$ will be disturbed to take the form

$$x = -x_0 + \eta\varepsilon \exp\left[\Omega t + i\left(my - nz\right)\right] + c.c, \tag{3.12}$$

where η is an amplitude factor to be found.

The stability analysis will determine a dispersion relation for the growth rate Ω as a function of the wavenumbers m,n, and the parameters x_0, σ, η.

Let us consider the simple case in which the magnetic field and rotation are both absent first in order to explain the stability analysis in some detail.

3.2.1 Standard Cartesian plume

Suppose that $\boldsymbol{\omega} = \mathbf{B}_0 = \mathbf{b}^{\dagger} = 0$ so that there is no magnetic field and no rotation. We find it convenient to define

$$\mathbf{u} = \left(-inu, -nv, w\right), \tag{3.13}$$

and express the perturbation equations in component form:

$$\Delta u - Dp = R\tilde{\Omega}u \tag{3.14}$$

$$\Delta v + mp = R\tilde{\Omega}v \tag{3.15}$$

$$\Delta w + T + C + n^2 p = R\left[\tilde{\Omega}w - in\bar{w}'u\right] \tag{3.16}$$

$$\Delta T - w = \sigma R\left[\tilde{\Omega}T - in\bar{T}'u\right] \tag{3.17}$$

$$\tilde{\Omega}C = 0 \tag{3.18}$$

$$Du + mv + w = 0 \tag{3.19}$$

Here we have defined

$$D = \frac{d}{dx}, \Delta = D^2 - m^2 - n^2, \tilde{\Omega} = \Omega - in\bar{w}(x) \tag{3.20}$$

Using equations (3.14)-(3.16) and (3.19), we derive the useful relation

$$\Delta p - T = 2Rin\bar{w}'u\ . \tag{3.21}$$

The boundary conditions can be stated as (see Eltayeb and Loper, 1991)

$$\begin{aligned}
&\text{(i) } u, v, w, T, p \to 0 \quad \text{as} \quad |x| \to \infty,\\
&\text{(ii) } u, v, w, T, p, DT \quad \text{are continuous across} \quad x = \pm x_0,\\
&(iii)\ \langle Dw \rangle_{\pm x_0} = \varepsilon\eta \left\langle \bar{C}(x) \right\rangle_{\pm x_0},\\
&\text{(iv) } -inu(x_0) = \Omega - in\bar{w}(x_0).
\end{aligned} \tag{3.22}$$

where the angular brackets in (3.22),(iii) denotes the jump defined by

$$\langle X \rangle_\alpha = X(\alpha - 0) - X(\alpha + 0). \tag{3.23}$$

Now that we have transformed the equations and boundary conditions in the form of ordinary differential equations with appropriate boundary conditions, we use the small parameter, R, in an expansion scheme:

$$f(\mathbf{x},t) = \sum_{s=0}^{\infty} f_s(\mathbf{x},t) R^s, \qquad \Omega = \sum_{s=1}^{\infty} \Omega_s R^{s-1}, \tag{3.24}$$

in which $f(\mathbf{x},t)$ stands for any of the perturbation variables and $\mathbf{x}$ is the position vector. The difference in the exponent of R from that in the expansion (4.17) used originally by Eltayeb and Loper (1991) is to accommodate the different time scale used here while preserving the notation for Ω.

The method of solution now proceeds by using the anstaz (3.24) into the equations (3.14)-(3.21) and the boundary conditions (3.22) and then equating the coefficients of the different powers of R to zero to obtain a hierarchy of systems of equations which can be solved seriatim. The standard Cartesian plume requires consideration of the first two such problems in order to close the eigenvalue problem. We shall now consider these two problems, but before we do that we note that equation (3.18) implies that

$$C = 0, \tag{3.25}$$

everywhere.

Problem 0

The coefficients of R^0 give the system

$$\Delta w_0 + T_0 + n^2 p_0 = 0, \tag{3.26}$$

$$\Delta T_0 - w_0 = 0, \tag{3.27}$$

$$\Delta p_0 - T_0 = 0, \tag{3.28}$$

$$\Delta u_0 - Dp_0 = 0, \tag{3.29}$$

$$\Delta v_0 + m p_0 = 0, \tag{3.30}$$

$$D u_0 + m v_0 + w_0 = 0. \tag{3.31}$$

This set of equations splits into two subsets. One subset is composed of equations (3.26)-(3.28), the other contains the rest of equations. The former set can be solved first. However, before we proceed to solve the equations, we note an important observation. The first set of equations involves the variables w_0, T_0, p_0 and the equations governing this subset contain only even derivatives. This means that the solutions of this set fall into two uncoupled categories of even and odd solutions in x. When we examine the second subset of equations, we find that v_0 has the same parity as w_0, T_0, p_0 while u_0 has a different parity. This means that one category is associated with w_0, T_0, p_0, v_0 even and u_0 odd. This will be referred to as the even solution or the varicose mode. The other solution is associated with odd w_0, T_0, p_0, v_0 and even u_0 and will be referred to as the odd solution or the sinuous (or meandering) mode.

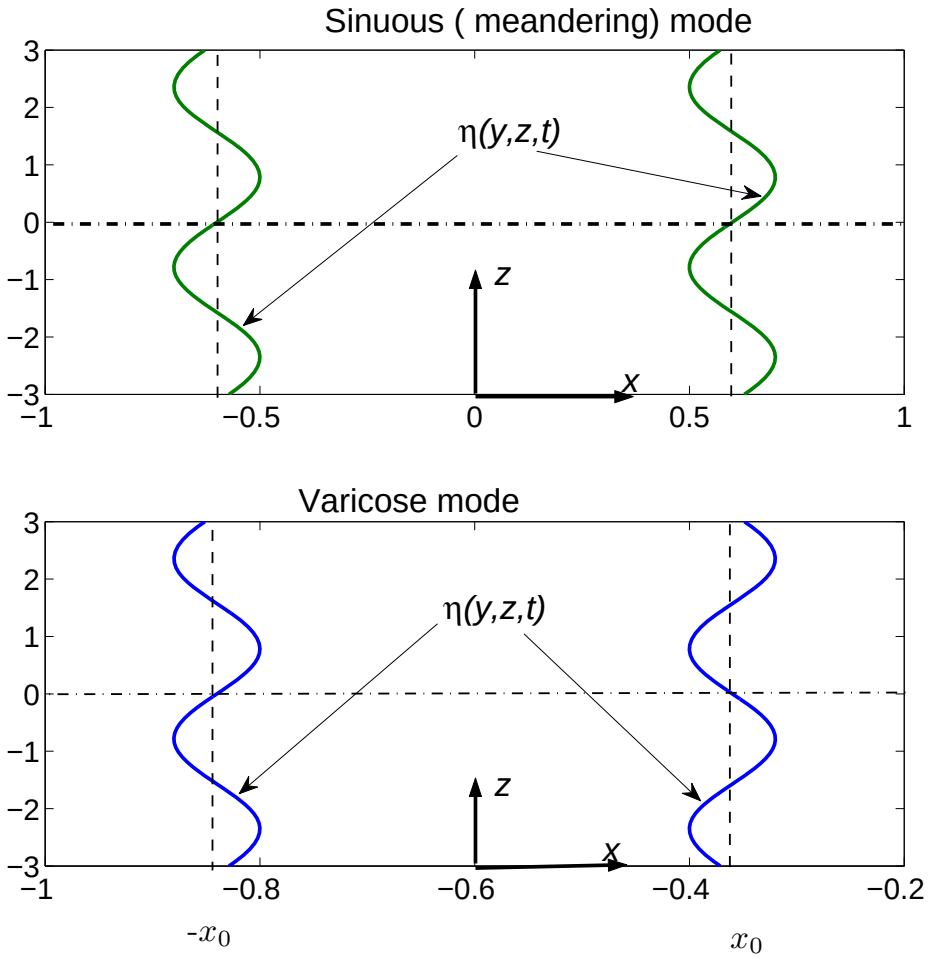

Figure 9. The profiles of the plume interfaces for the two types of solutions of the perturbation equations

The consequence of the parity property is that the two interfaces are either in-phase corresponding to the sinuous mode in which case

$$\eta = 1 \tag{3.32}$$

or out-of-phase giving a varicose mode and then

$$\eta = -1 \tag{3.33}$$

The two forms of undulations are illustrated in figure 9.

The significance of the parity property is that we can solve the problem in the semi-infinite interval $[0,\infty)$ using the parity conditions at $x=0$ and the boundary conditions at $x=x_0$. We find that

when $0 \le x < x_0$:

$$\{w_0, T_0, p_0, v_0\} = \sum_{j=1}^{3} A_j \left\{\mu_j^3, \mu_j^2, \mu_j, -\lambda_j\right\} e^{-\lambda_j x_0} \begin{cases} \cosh\left[\lambda_j x\right]; & \text{for varicose mode} \\ \sinh\left[\lambda_j x\right]; & \text{for sinuous mode} \end{cases} \tag{3.34}$$

$$u_0 = \sum_{j=1}^{3} A_j \lambda_j e^{-\lambda_j x_0} \begin{cases} \sinh\left[\lambda_j x\right]; & \text{for varicose mode} \\ \cosh\left[\lambda_j x\right]; & \text{for sinuous mode} \end{cases}. \tag{3.35}$$

and when $x > x_0$:

$$\{w_0, T_0, p_0, v_0\} = \sum_{j=1}^{3} A_j \left\{\mu_j^3, \mu_j^2, \mu_j, -\lambda_j\right\} e^{-\lambda_j x} \begin{cases} \cosh\left[\lambda x_0\right]; & \text{for varicose mode}, \\ \sinh\left[\lambda x_0\right]; & \text{for sinuous mode} \end{cases} \tag{3.36}$$

$$u_0 = -\sum_{j=1}^{3} A_j \lambda_j e^{-\lambda_j x} \begin{cases} \cosh\left[\lambda_j x_0\right]; & \text{for varicose mode} \\ \sinh\left[\lambda_j x_0\right]; & \text{for sinuous mode} \end{cases}, \tag{3.37}$$

where

$$A_j = \frac{\mu_j^2}{2\lambda_j\left[2\mu_j + 3n^2\right]}, \tag{3.38}$$

$$\mu_j^3 + \mu_j + n^2 = 0, \quad \lambda_j = \left(\mu_j + m^2 + n^2\right)^{1/2} \tag{3.39}$$

The expression for the growth rate is obtained from the boundary condition (3.22),(iv) as

$$\frac{\Omega_1}{in} = \bar{w}\left(x_0\right) \pm \frac{1}{2}\sum_{j=1}^{3} A_j \lambda_j e^{-2\lambda_j x_0} \tag{3.40}$$

The solution of problem 0 is now complete. The growth rate Ω_1, as in (3.40), is purely imaginary indicating that the disturbance is neutral at this degree of approximation. In order to determine the stability we must consider the next order problem.

Problem 1

The coefficients of R^1 give

$$\Delta w_1 + T_1 + n^2 p_1 = R\left[\tilde{\Omega}_1 w_0 - in\bar{w}' u_0\right] \tag{3.41}$$

$$\Delta T_1 - w_1 = \sigma R\left[\tilde{\Omega}_1 T_0 - in\bar{T}' u_0\right] \tag{3.42}$$

$$\Delta p_1 - T_1 = 2Rin\bar{w}' u_0 \tag{3.43}$$

$$\Delta u_1 - Dp_1 = R\tilde{\Omega}_1 u_0 \tag{3.44}$$

$$\Delta v_1 + mp_1 = R\tilde{\Omega}_1 v_0 \tag{3.45}$$

$$Du_1 + mv_1 + w_1 = 0 \tag{3.46}$$

The boundary conditions take the form

$$\begin{aligned} &\text{(i)} u_1, v_1, w_1, T_1, p_1 \to 0 \quad \text{as} \quad |x| \to \infty, \\ &\text{(ii)}\ u_1, v_1, w_1, T_1, p_1, DT_1, \mathrm{D}w_1 \ \text{ are continuous across } \ x = \pm x_0, \\ &\text{(iii)}\ -\mathrm{i}nu_1(x_0) = \Omega_2. \end{aligned} \tag{3.47}$$

This system can be solved in the form of complementary function and particular integral for each variable and the application of the boundary conditions yields a dispersion relation for the growth rate Ω_2. Alternatively, a solvability condition can be derived to obtain an expression for Ω_2. The calculations are lengthy and laborious but straightforward. It can be written that

$$\Omega_2^P = c_0^P(m, n; x_0) + \sigma c_1^P(m, n; x_0), \tag{3.48}$$

so that the growth rate is linear in Prandtl number. Here the P is a parameter denoting parity so that there are two expressions one for the varicose mode and the other for the sinuous mode. The detailed derivation of (3.48) can be found in Eltayeb and Loper (1994) or as a special case of Eltayeb *et al*. (2005) Appendix A.

It turned out that the expressions c_0^P, c_1^P are both real so that Ω_2 represents growth if $\Omega_2 > 0$ giving instability or decay when $\Omega_2 < 0$ representing stability. For every fixed pair (σ, x_0), Ω_2 is maximized over the wavenumber pair (m, n) to identify the maximum growth rate $\Omega_c(\sigma, x_0)$ and the associated wavenumbers m_c, n_c. Once the wavenumbers of the preferred mode are found, we can calculate Ω_{1c} to obtain the phase speeds

$$U_z = \Omega_{1c} / \mathrm{i}n_c; \qquad U_y = n_c U_z / m_c; \quad (m \neq 0) \tag{3.49}$$

The set $(\Omega_c, m_c, n_c, U_z)$ defines the preferred mode of instability. It is found that the Cartesian plume is unstable for all values of σ, x_0 even when $x_0 \to \infty$.

The vertical wavenumber n_c of the preferred mode is always non-zero. The horizontal wavenumber, m_c, can take non-zero values and the instability is 3-dimensional in which case the waves propagate in a direction inclined to the vertical. If, however, $m_c = 0$ and the instability is 2-dimensional, the waves propagate vertically. The instability then takes one of four types of mode: vertical varicose, V_v, oblique varicose, V_o, vertical sinuous, S_v, and oblique sinuous, S_o. The instability is summarised in a stability regime in Figure 10.

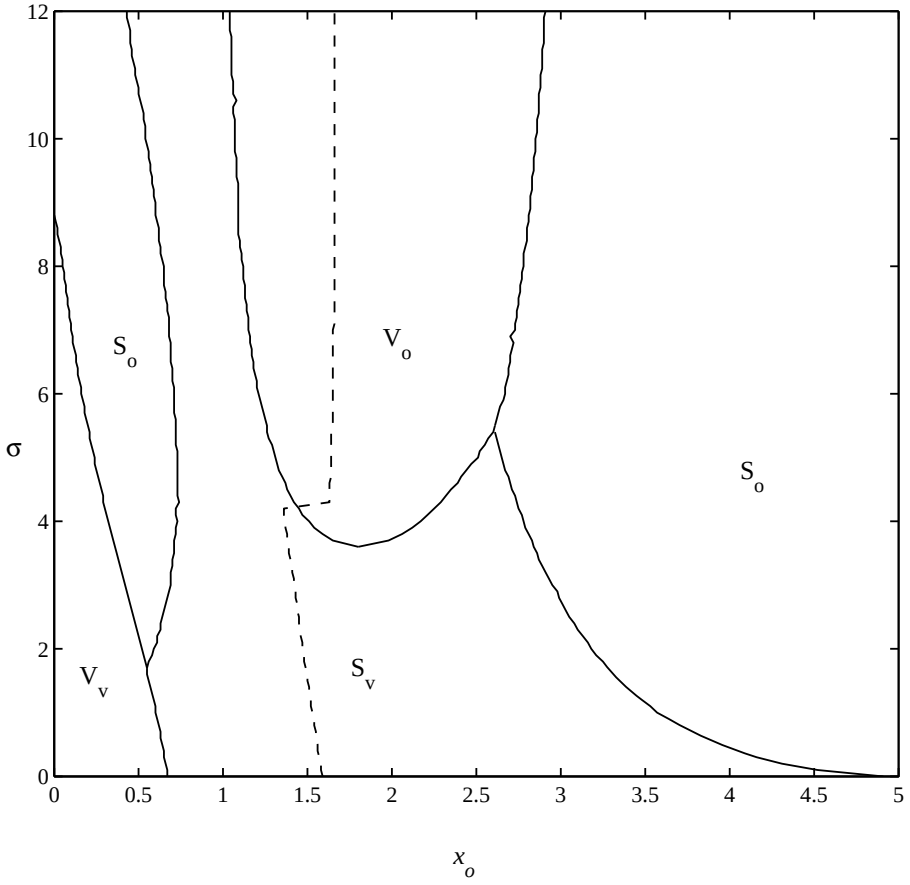

Figure 10. The regions of mode preference for the instability of the Standard Cartesian plume. The broken curve represents the position of the overall maximum growth rate for given σ. Note that the values of x_0 vary between 1.4 and 1.7.

The growth, Ω_c, of the preferred mode is a function of the two parameters σ, x_0. It is interesting to examine its dependence on these two parameters. For fixed σ, Ω_c increases as x_0 increases from 0 reaching a maximum, $\Omega_{c\max}$, before it decreases rapidly at first and then slowly but always remaining positive as $x_0 \to \infty$. $\Omega_{c\max}$ varies between 1.4 and 1.7. The smaller values occur for small σ and belong to the sinuous vertical mode, S_v, while the larger values occur for large σ and the oblique varicose mode (see Figure 11). As σ increases from 0, $\Omega_{c\max}$ initially decreases but as σ exceeds 4.0 it begins to increase with the increase of σ. However, as x_0 increases for large values, the growth rate decreases with σ.

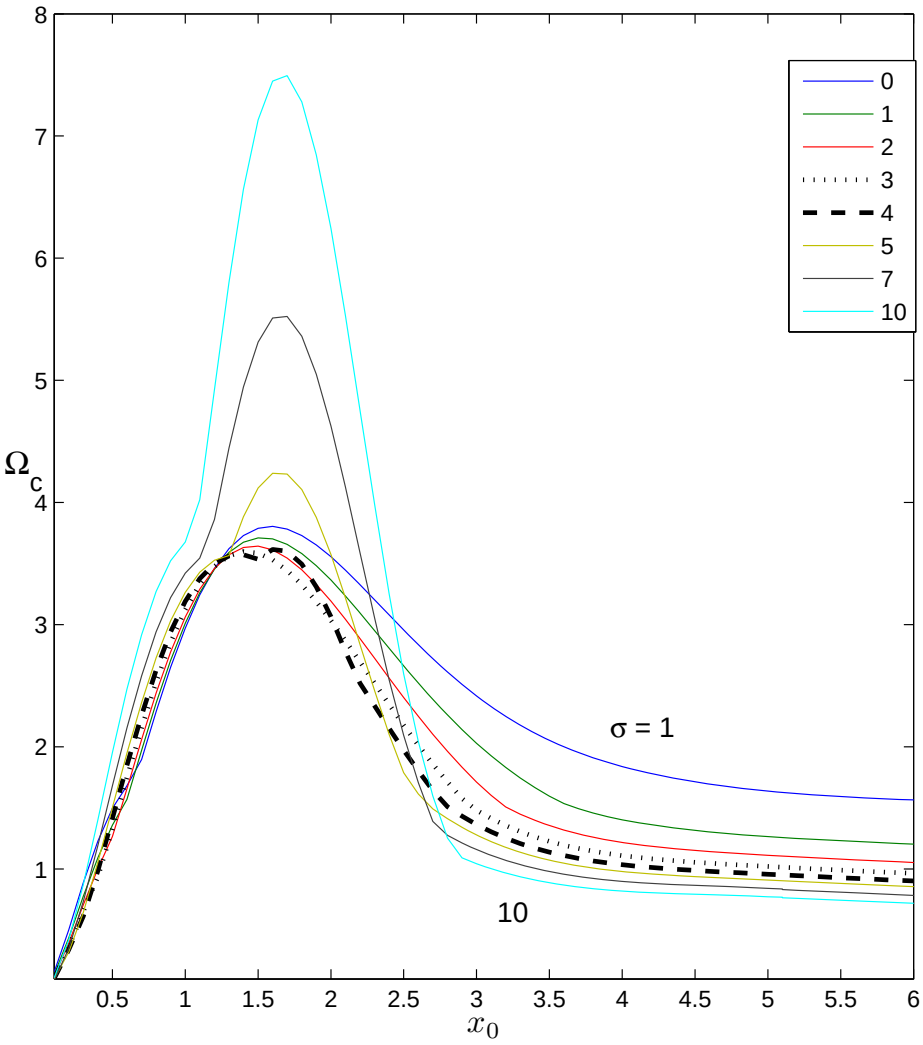

Figure 11. The dependence of the growth rate, Ω_c, of the preferred mode on the thickness of the plume for different values of σ. Note that the dotted curve corresponds to σ = 3.0 and the broken one to σ = 4.0.

3.2.2. Magnetic Cartesian plume

When a magnetic field is introduced into the Cartesian plume, the relevant equations are obtained from (2.31)-(2.35) by setting $\omega_H = \omega_z = 0$. The boundary conditions are given by (3.22) with the addition of the continuity of the magnetic field everywhere. For detailed expressions for the equations and boundary conditions see Eltayeb et al. (2004, 2005).

The basic state is the same as for the standard Cartesian plume with the addition of the uniform ambient magnetic field $\mathbf{B_0}$. The solution has the same structure as that

obtained for the Standard Cartesian plume with the zeroth order solution taking the form

$$\{w_0, T_0, p_0, b_0\}$$

$$= \sum_{j=1}^{3} A_j \left\{\mu_j^3, \mu_j^2, \mu_j, -\mathrm{i}\delta\mu_j^2\right\} e^{-\lambda_j x_0} \begin{cases} \cosh\left[\lambda_j x\right]; & \text{for varicose mode} \\ \sinh\left[\lambda_j x\right]; & \text{for sinuous mode} \end{cases} \tag{3.50}$$

$$\{u_0, b_{x0}\} = \sum_{j=1}^{3} A_j \lambda_j \frac{\left\{\mu_j^2, -\mathrm{i}\delta\mu_j\right\}}{\mu_j^2 + \delta^2 Q} e^{-\lambda_j x_0} \begin{cases} \sinh\left[\lambda_j x\right]; & \text{for varicose mode} \\ \cosh\left[\lambda_j x\right]; & \text{for sinuous mode} \end{cases} \tag{3.51}$$

For $0 \le x < x_0$; and

$$\{w_0, T_0, p_0, b_0\}$$

$$= \sum_{j=1}^{3} A_j \left\{\mu_j^3, \mu_j^2, \mu_j, -\mathrm{i}\delta\mu_j\right\} e^{-\lambda_j x} \begin{cases} \cosh\left[\lambda x_0\right]; & \text{for varicose mode} \\ \sinh\left[\lambda x_0\right]; & \text{for sinuous mode} \end{cases} \tag{3.52}$$

$$\{u_0, b_{x0}\} = -\sum_{j=1}^{3} A_j \lambda_j \frac{\left\{\mu_j^2, -\mathrm{i}\delta\mu_j\right\}}{\mu_j^2 + \delta^2 Q} e^{-\lambda_j x} \begin{cases} \cosh\left[\lambda_j x_0\right]; & \text{for varicose mode} \\ \sinh\left[\lambda_j x_0\right]; & \text{for sinuous mode} \end{cases} \tag{3.53}$$

for $x > x_0$. Here we have defined

$$A_j = \frac{\mu_j^2 + \delta^2 Q}{2\lambda_j \left[2\mu_j \left(1 + \delta^2 Q\right) + 3n^2\right]}, \tag{3.54}$$

$$\mu_j^3 + \mu_j \left(1 + \delta^2 Q\right) + n^2 = 0, \quad \lambda_j = \left(\mu_j + m^2 + n^2\right)^{1/2}, \tag{3.55}$$

$$Q = \frac{Q_c}{1 + B_v^2}. \tag{3.56}$$

The next order problem leads to a solvability condition giving a real growth rate Ω_2:

$$\Omega_2\left(m, n; x_0, \sigma, \sigma_m, Q\right) = \Omega_{20}\left(m, n; x_0, Q\right) + \sigma\Omega_{2i}\left(m, n; x_0, Q\right) + \sigma_m \Omega_{2m}\left(m, n; x_0, Q\right) \tag{3.57}$$

The instability problem gives rise to the same four modes of instability encountered in the Standard Cartesian plume but here affected by the presence of the magnetic filed, as represented by Q, and by magnetic diffusion, as represented by σ_m. We will discuss the main features on the instability introduced by the field.

The unexpected result here is that the magnetic field is unable to stabilise the system, although it tends to decrease the magnitude of the growth rate. Indeed, it is found that the system is unstable for all values of the parameters $x_0, \sigma, \sigma_m, Qc$, although the regime diagrams suffer some changes of mode arrangement. A sample is given in figure 12 .

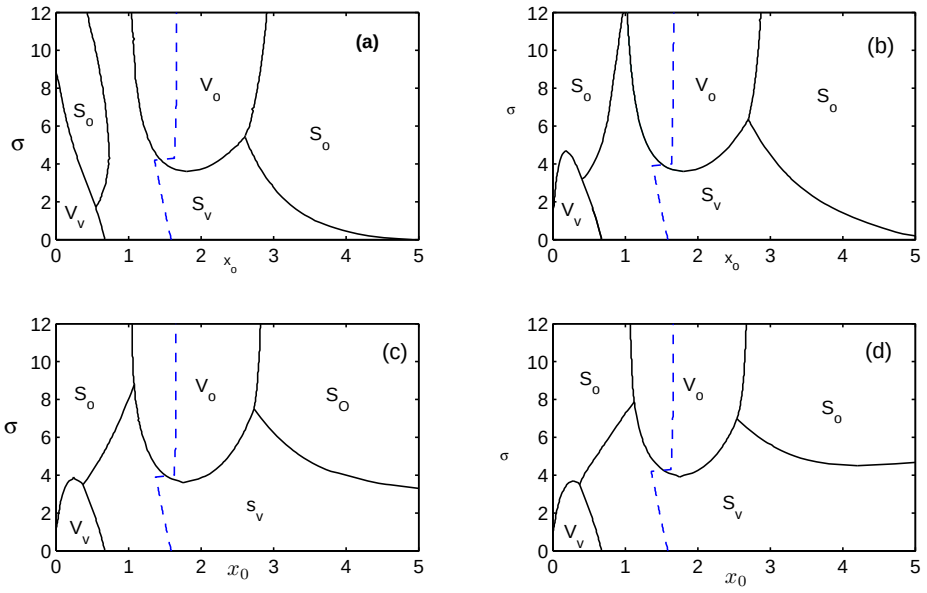

Figure12. The regime diagram in the $x_0 - \sigma$ plane illustrating the regions where the different modes are preferred for a horizontal magnetic field (B_v = 0.0) when $\sigma_m = 0.0$. (a), (b), (c), and (d) correspond to *Qc* taking the values 0.0, 0.20, 1.0 and 100.0, respectively. The discontinuous curve refers to the position of the global maximum with growth rate Ω_{max} We note that the horizontal magnetic field tends to suppress the vertical modes for small values (≤ 1.2) of x_0 and enhance them for large x_0. The vertical wavenumber is about unity for the vertical mode when x_0 is small and is less than unity for all other modes. The horizontal wavenumber, on the other hand, is rarely in excess of 0.4.

The inclination of the field plays an important role in the stability problem. The introduction of a vertical component to a model with a horizontal field introduces two factors: (i) it suppresses the vertical sinuous mode for moderate to large values of x_0 at the expense of the oblique sinuous mode and suppresses the oblique sinuous mode for small values of x_0 at the expense of the vertical sinuous mode. There is very little influence on the varicose mode (see Figure 13) and (ii) for certain moderate values of field inclination, the growth rate is enhanced (see figure 14). The influence of magnetic diffusion is always stabilizing (see figure 15). However, its effect on the type of unstable mode depends on the strength of the magnetic field. For small fields, it suppresses the vertical sinuous mode present for small values of x_0, but it enhances the same mode for large amplitudes of the field (see figure 16).

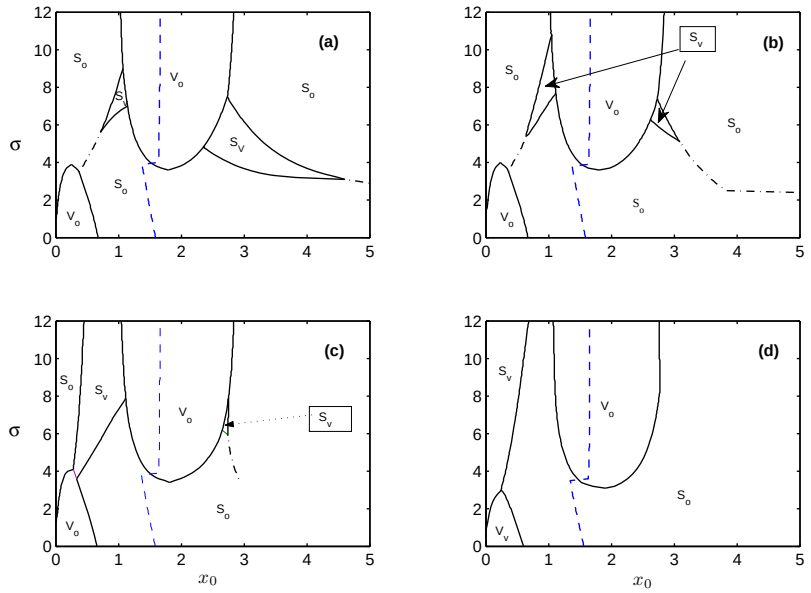

Figure 13. The x_0-σ regime diagram in the case Qc=1.0, σ_m =0.0 illustrating the effect of increasing the vertical component of field as follows: (*a*) B_v = 0.02, (*b*) B_v = 0.1, (*c*) B_v = 0.2, (*d*) B_v = 0.5. Compare (a) with Figure 4(c) for B_v = 0.0. While the varicose vertical mode disappears once the vertical field is non-zero, the regions of preference of the sinuous mode are only partly suppressed for small vertical fields as in (a). Further increase in B_v leads to further suppression of the sinuous vertical mode for large x_0 but at the same time a new sinuous vertical mode appears for smaller (less than about 1.2) x_0 and $\sigma \geq 4.0$. This new vertical mode region expands into smaller x_0 direction and eventually extends to the region for oblique varicose mode present for small x_0 (see (c)). Further increase of B_v to about 0.4, leads to the migration of this region towards the σ-axis and eventually to the complete disappearance of the vertical mode.

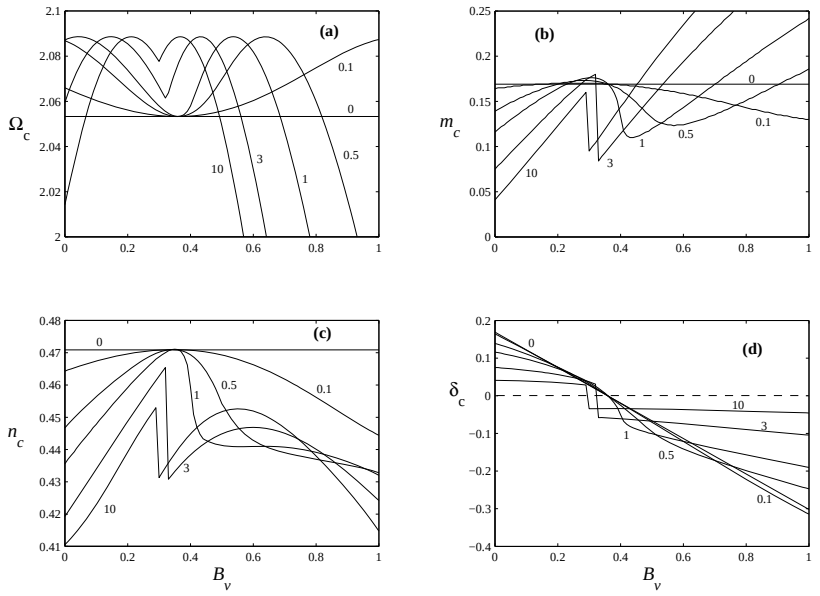

Figure 14. The critical mode parameters ($\Omega_c, m_c, n_c, \delta_c$) as a function of the vertical field inclination B_v for x_o = 1.8, σ = 5.0, σ_m = 0.0 for different values of Qc. This is a case in which the vertical field enhances the growth rate in a certain range of inclination. We observe the changing profile of the growth rate as Qc increases.

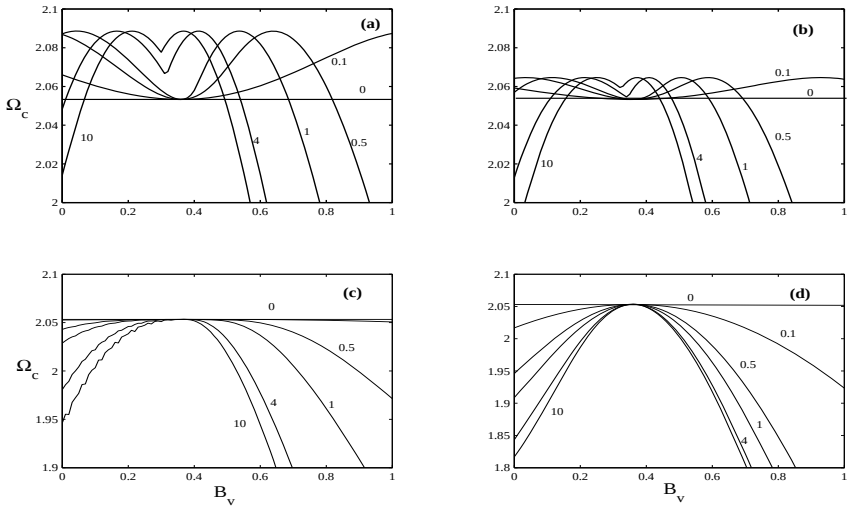

Figure 15. An illustration of the conflicting influences of the vertical field and magnetic diffusion on the preferred mode of convection as experienced at a point (1.8, 5.0) in the oblique varicose mode region in the regime diagram. Here (a) σ_m = 0.0, (b) σ_m = 0.5, (c) σ_m = 1.0, (d) σ_m = 4.0, and the Arabic numerals refer to the value of *Qc*. We note that in the absence of magnetic diffusion (i.e. when σ_m= 0) the vertical field component can enhance instability (as in (a)) but an increase in magnetic diffusion acts to suppress this destabilizing influence so that when σ_m is about unity, the enhancement of growth rate by the vertical component of field has completely disappeared and thereafter the maximum possible growth rate for field strengths is the value in the absence of the field. Such a value can only occur for a certain value of B_v which depends on σ. The wavenumbers experience a jump for the modes with the two local maxima. However, for the cases which touch the line for *Qc* = 0 the wavenumbers vary continuously (see Figure 14).

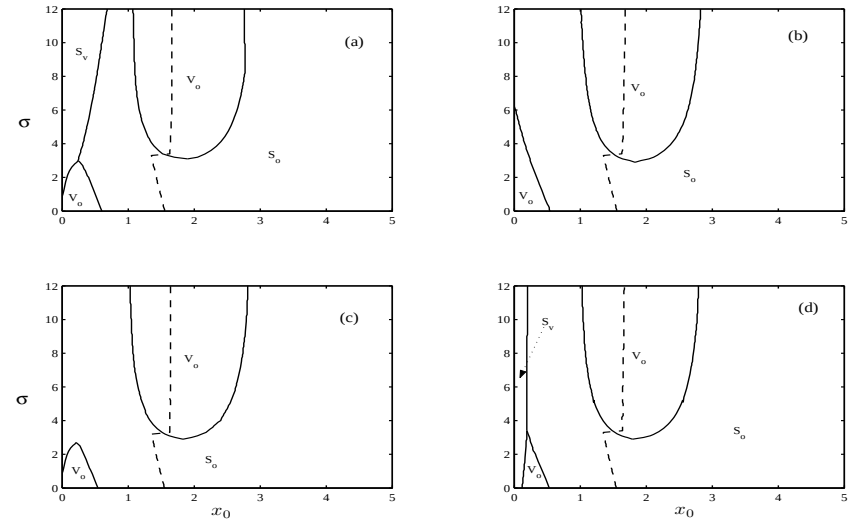

Figure 16. . The influence of magnetic diffusion on the x_o -σ regime diagram when the field is inclined to the vertical. Here B_v = 0.5 and (a) *Qc* = 1.0, σ_m = 0.0, (b) *Qc* = 1.0, σ_m = 5.0, (c) *Qc* = 10.0, σ_m = 0.0 (d) *Qc* = 10.0, σ_m = 5.0. The increase of magnetic diffusion here suppresses the vertical sinuous mode when *Qc* is small and gives rise to it for small x_0 when *Qc* is large. The discontinuous-dotted curve again refers to the position of the overall maximum.

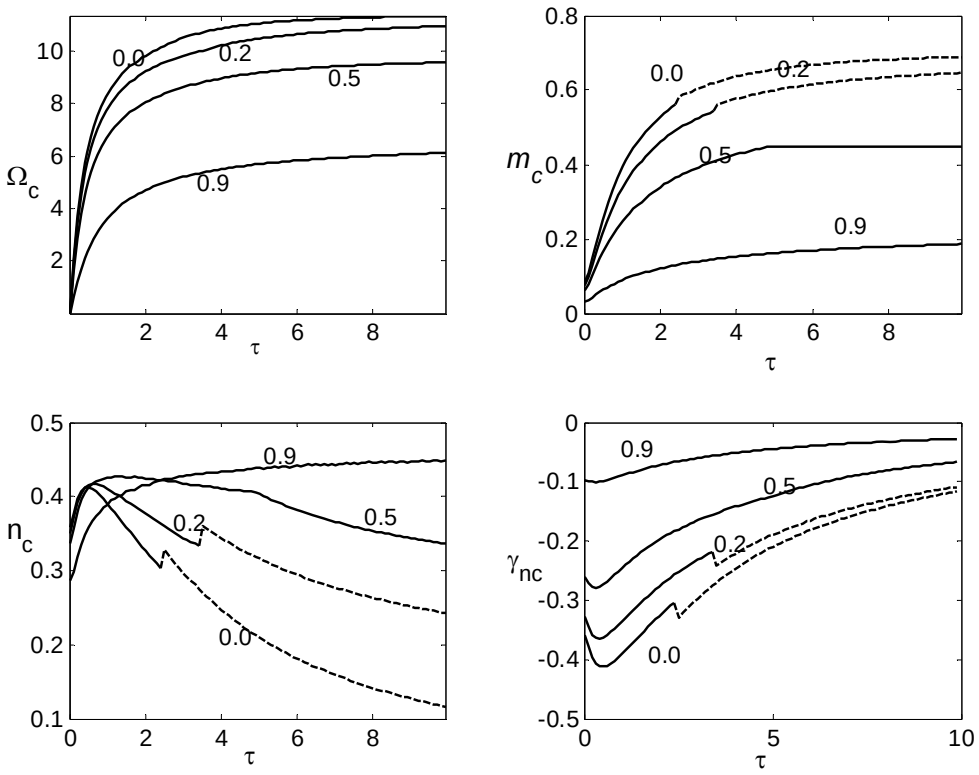

Figure 17. Illustration of the dependence of the critical mode of the rotating Cartesian plume on the Taylor number, τ^2, and the direction of the rotation vector, as measured by ω_H. The jump in the wavenumbers indicates a change of mode from varicose for small τ to sinuous for large τ. The figure is drawn for $x_0 = 3.0$ and four values of ω_H as labelled. The change of parity depends on the value of x_0: there is no change of mode for small x_0 (<~1.5) in which case the varicose mode is preferred. Note that γ_{nc} is always negative.

3.2.3 Rotating Cartesian plume

Here we examine the influence of rotation acting alone on the Cartesian plume (Eltayeb and Hamza 1998, Classen *et al*. 1999). It is found that the two Prandtl numbers do not enter the stability problem here. The zeroth order problem here gives the relation

$$\frac{\Omega_1}{in} = \bar{w}\left(x_0\right) + \sum_{j=1}^{3} \frac{\mu_j^2}{2\mu_j + 3n^2} \cosh\left(\lambda_j x_0\right) e^{-\lambda_j x_0} + m\gamma\tau \sum_{j=1}^{3} \frac{\mu_j^3}{\lambda_j\left(2\mu_j + 3n^2\right)} \cosh\left(\lambda_j x_0\right) e^{-\lambda_j x_0} \tag{3.58}$$

in which

$$\gamma = m\omega_H - n\omega_z \tag{3.59}$$

In contrast with the pervious the two cases, the expression for $\left(\Omega_1 / in\right)$ is complex and hence the stability of the problem can be decided at this level of approximation. It

is noteworthy that the new term that gives $\left(\Omega_1 / in\right)$ an imaginary part is proportional to the horizontal wavenumber m and rotation rate. This means that *the presence of rotation increases the order of magnitude of the growth rate from* $O\left(R\right)$ *in the absence of rotation to* $O\left(1\right)$ *in its presence.* This means that rotation enhances the instability of the plume. An increase in the horizontal component, ω_H, of rotation tends to inhibit instability but the system is always unstable (Figure 17). It is also found that the horizontal component of rotation tends to suppress the sinuous mode for small values of τ (Figure 18).

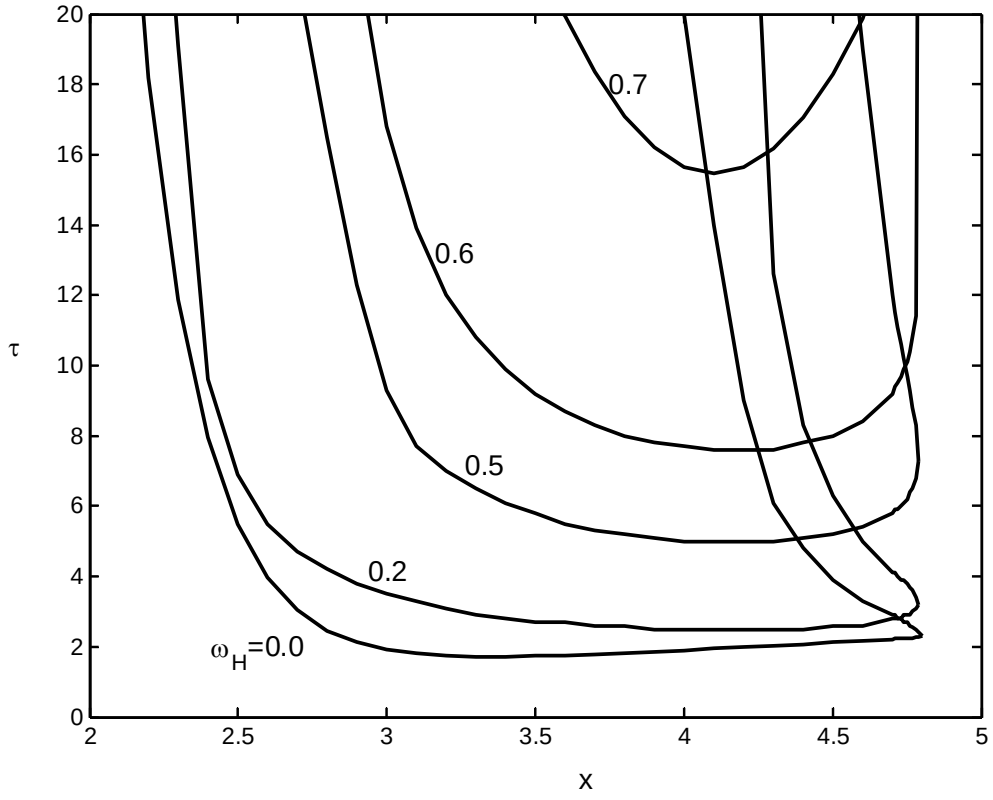

Figure 18. The regime diagram for the stability of the rotating Cartesian plume in the (x_0, τ) plane. The curves divide the plane into regions where the sinuous mode is preferred (within the curve) and another region where the varicose mode is preferred (outside). The curves for different values of ω_H, as labelled, are superimposed. Note the tendency of the horizontal component of rotation to suppress the sinuous mode for small τ.

3.2.4. Rotating magnetic Cartesian plume

The rotating magnetic plume provides an example of a compositional plume under the simultaneous action of magnetic field and rotation. We have seen that the magnetic field acting alone tends to inhibit instability but can also, by its vertical component, promote instability. However, the growth rate remains $O\left(R\right)$, as in the absence of the

field. The presence of rotation on the other hand, increases the order of the growth rate to $O(1)$ and instability is present at that order for all values of the thickness of the plume and is independent of the Prandtl number.

The combined action of field and rotation is primarily dominated by the presence of rotation. Instability is present for all values of the parameters and the growth rate has $O(1)$ values. The instability is independent of both Prandtl numbers σ, σ_m. However, the interaction of the two constraints has its significance. The conflicting influences of the vertical component of magnetic field and the horizontal component of rotation is illustrated in Figure (figure 19).

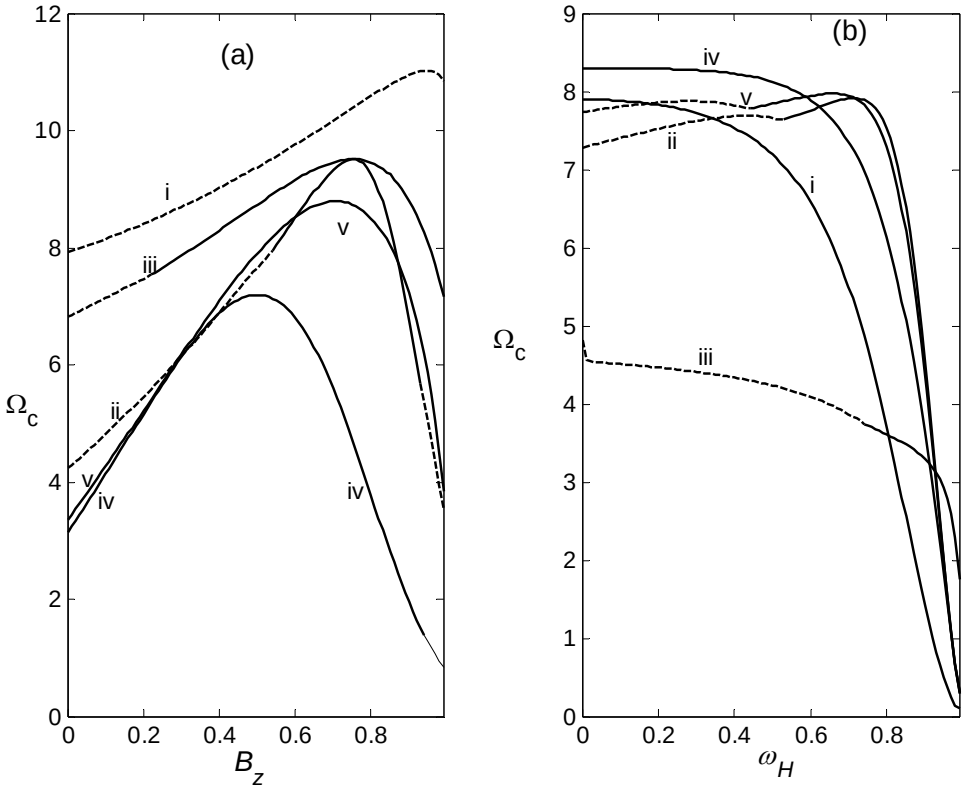

Figure 19. The dependence of the critical growth rate on the inclinations of the magnetic field and rotation vector. The continuous (discontinuous) curves refer to the varicose (sinuous) mode. The labels i-v, respectively, refer to : in (a) (Qc, τ, ω_H) taking the values (5.0, 1.0, 0.5), (5.0, 5.0, 0.5), (5.0, 5.0, 0.0), (2.0, 2.0, 0.5), (4.0, 4.0, 0.5) and in (b) (Qc, τ, B_z) corresponding to (1.0, 5.0, 0.0), (5.0, 5.0, 0.5), (1.0, 5.0, 0.5), (5.0, 1.0, 0.5), (5.0, 1.0, 0.0).

3.3 Cylindrical plume

When a plume of cylindrical cross-section of radius, r_0, is studied, the results are qualitatively similar to those obtained for the Cartesian plume with the main difference being that the horizontal wavenumber is an integer (see Eltayeb and Loper 1997).

3.4 **Helicity and α -effect** of the Cartesian plume

The unstable motion of compositional plumes may be relevant to the Earth's outer core. Motions in the iron-rich molten outer core of the Earth interact with the magnetic filed there to produce electromotive force (e.m.f) that helps regenerate the magnetic field of the earth. This process is called the geodynamo.

It is known that the helicity of the small–scale of motions is conducive to dynamo action particularly when the magnetic Reynolds number is small. Here the helicity is defined by

$$H\left(x\right)=\left\langle\left\langle \mathbf{u}.\left(\nabla\times\mathbf{u}\right)\right\rangle\right\rangle \tag{3.60}$$

where the double angular brackets denote averaging over y and z. It can be shown that

$$H\left(x\right)=n\,\mathrm{Re}\left[nu^{*}v-mw^{*}u+\frac{1}{2}\left(vDw^{*}-w^{*}Dv\right)\right] \tag{3.61}$$

Noting the parity of solutions of the Cartesian plume, we clearly see that $H\left(x\right)$ is an odd function of x with the consequence that the total helicity, H_{tot}, defined by

$$H_{tot}=\int_{-\infty}^{\infty}H\left(x\right)dx \tag{3.62}$$

vanishes whatever the values of the parameters of the problem.

However, the cylindrical plume possesses a helicity function that has no definite parity (Eltayeb 1999) and as a result the total helicity is non-zero.

Another important property of the small-scale motions in an electrically conducting fluid is the $\alpha-$effect. This can be defined simply by assuming the the magnetic field and velocity fields have mean parts $\mathbf{B},\mathbf{U}$ depending on a large scale L_s and fluctuating parts $\mathbf{b},\mathbf{u}$ which vary on a short length scale ℓ. The equation of induction (2.14) then gives

$$\sigma_m\frac{\partial\mathbf{B}}{\partial t}+\sigma_m\frac{\partial\mathbf{b}}{\partial t}=\sigma_m R\nabla\times\left[\mathbf{U}\times\mathbf{B}+\mathbf{u}\times\mathbf{B}+\mathbf{U}\times\mathbf{b}+\mathbf{u}\times\mathbf{b}\right]+\nabla^2\mathbf{B}+\nabla^2\mathbf{b} \tag{3.63}$$

If we average this equation over the two coordinates x, y, we obtain

$$\sigma_m\frac{\partial\mathbf{B}}{\partial t}=\sigma_m R\nabla\times\left[\mathbf{U}\times\mathbf{B}\right]+\sigma_m R\nabla\times\left[\left\langle\left\langle\mathbf{u}\times\mathbf{b}\right\rangle\right\rangle\right]+\nabla^2\mathbf{B} \tag{3.64}$$

The quantity $\left\langle\left\langle\mathbf{u}\times\mathbf{b}\right\rangle\right\rangle$ is the mean electromotive force due to the fluctuations at small length scale i.e. the small-scale motions

$$\mathbf{E}=\left\langle\left\langle\mathbf{u}\times\mathbf{b}\right\rangle\right\rangle \tag{3.65}$$

This quantity can be evaluated from the perturbation equations and expressed in the form

$$E_i = \bar{\alpha} f_{ij} B_j ; \quad i, j = 1,2,3. \tag{3.66}$$

using tensor notation for the components of vectors (Malkus and proctor 1975). Thus the perturbations can produce a source in the direction of the ambient field and hence may help maintain the mean magnetic field. Such an effect is known as the α – effect. The mean electromotive (e.m.f) force **E** is a measure of it. We define the total e.m.f. by

$$E(x) = \mathbf{E}.\hat{\mathbf{B}}_0 = B_H E_y + B_z E_z \tag{3.67}$$

$$E_y = n \,\mathrm{Im}\left(w^* b_x + u^* b_z\right), \quad E_z = n \,\mathrm{Im}\left(u^* b_y + v^* b_x\right) \tag{3.68}$$

We also find that $E(x)$ is odd in x . The behaviour of the helicity and α – effect functions is illustrated in Figure 20. Note the discontinuity of the vorticity at the interfaces due to its dependence on $\partial w^{\dagger} / \partial x$.

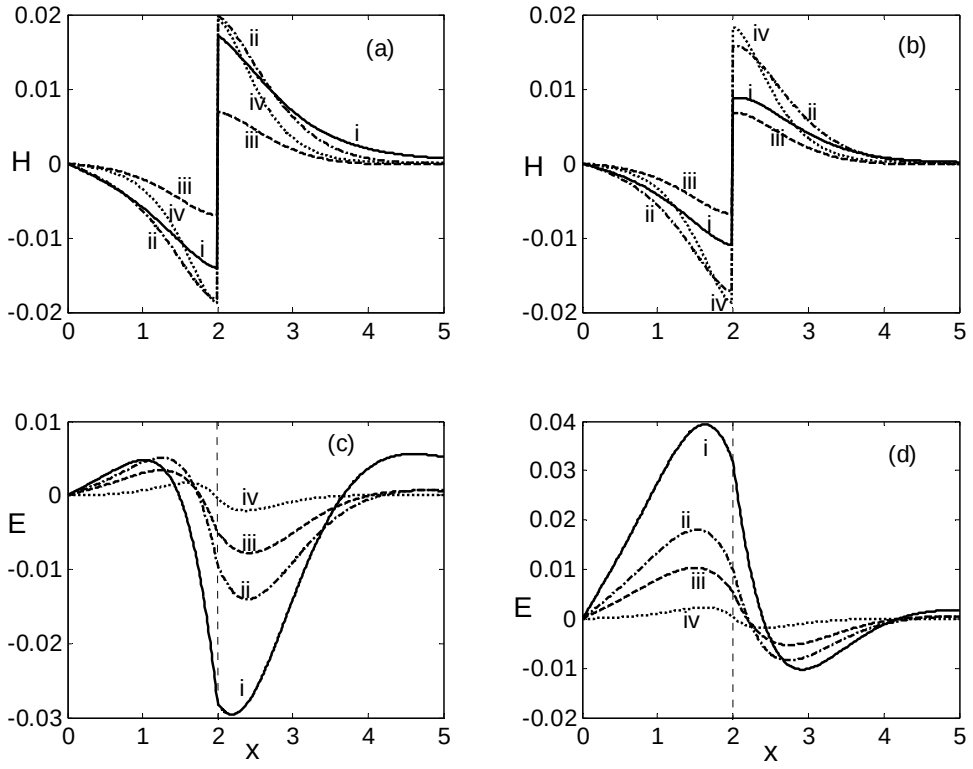

Figure 20. The helicity, *H*, and α –effect, *E*, for a sample of the parameters: $x_0 = 2.0$, *Qc* =1.0, τ =0.5, $B_z = 0.2$, $\omega_T = 0.5$. Figures (a) and (c) correspond to *P*= 1.0 and (b) and (d) refer to *P* = -1.0. The curves i – iv correspond, respectively, to the wave number pair (*m*, *n*) taking the values (0.2,0.5), (0.5,0.2), (0.5,0.5), (1.0,1.0). We see that the change in parity influences the α –effect more than the helicity.

However, the helicity and e.m.f. the cylindrical model do not possess any parity and hence their total values are non-zero. See Eltayeb (1999).

4. Two interacting plumes

It is quite possible that plumes may not always occur in isolation and it is of interest to examine their interaction. In particular, the layer of a few hundred kilometres thickness believed to exist at the inner-outer core interface of the Earth composed of mixed heavy iron-rich solid crystals and light fluid releases its light fluid component in the form of plumes which rise into the outer fluid core.

In order to gain some understanding of the interaction of these plumes, we consider a pair of them here in the absence of rotation and magnetic field.

Consider a basic concentration of light material of the form

$$\bar{C} = \begin{cases} 0 & \text{if} \quad x < -x_0 \\ 1 & \text{if} \quad -x_0 < x < x_0 \\ 0 & \text{if} \quad x_0 < x < c_1 \\ \Gamma & \text{if} \quad c_1 < x < d_1 \\ 0 & \text{if} \quad x > d_1 \end{cases}, \tag{4.1}$$

where

$$c_1 = x_0 + d, \quad d_1 = x_0 + d + 2x_1 \tag{4.2}$$

The geometry of the two-plume model is illustrated in Figure 21.

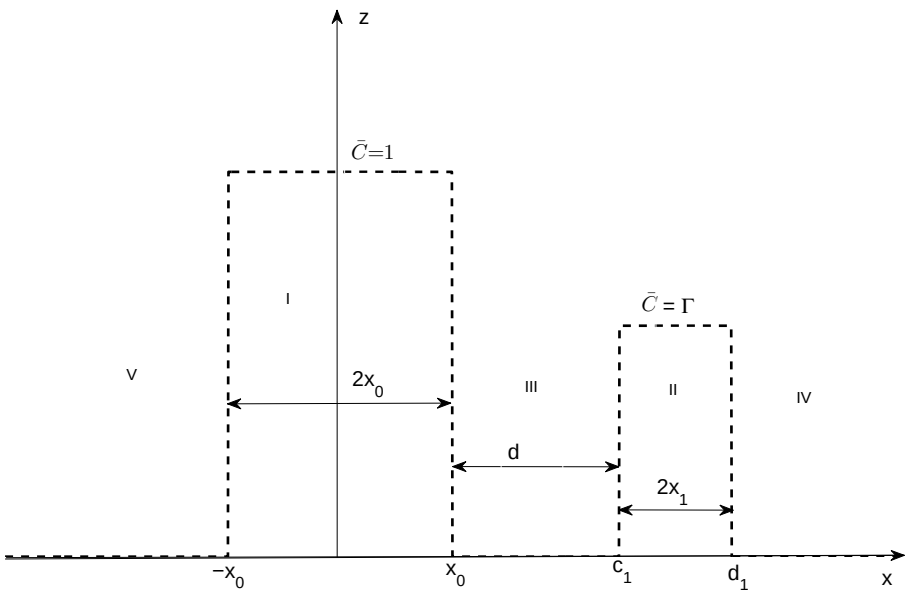

Figure 21. The profile of the basic concentration of the light material giving rise to two plumes. The two plumes divide the fluid into five regions as labelled. Region I is the primary plume, thickness $2x_0$, while region II is the secondary plume, thickness $2x_1$.

The basic state equations (2.27)-(2.30) are solved with $\bar{C}$ given by (4.1) subject to the conditions that Y , dY/dx

$$\begin{aligned} Y_5 &= A_5 \exp(kx), && x < -x_0, \\ Y_1 &= A_1 \cosh(kx) + B_1 \sinh(kx) - 1, && -x_0 < x < x_0, \\ Y_3 &= A_3 \cosh(kx) + B_3 \sinh(kx), && x_0 < x < c_1, \\ Y_2 &= A_2 \cosh(kx) + B_2 \sinh(kx) - \Gamma, && c_1 < x < d_1, \\ Y_4 &= A_4 \exp(-kx), && x > d_1, \end{aligned} \tag{4.3}$$

in which

$$\begin{aligned} A_1 &= -\Gamma e^{-kq} \sinh(kx_1) + e^{-kx_0}, & B_1 &= -\Gamma e^{-kq} \sinh(kx_1), \\ A_2 &= \Gamma e^{-kx_1} \cosh(kq) - \sinh(kx_0), & B_2 &= -\Gamma e^{-kx_1} \sinh(kq) + \sinh(kx_0), \\ A_3 &= -\Gamma e^{-kq} \sinh(kx_1) - \sinh(kx_0), & B_3 &= -\Gamma e^{-kq} \sinh(kx_1) + \sinh(kx_0), \\ A_4 &= -\Gamma e^{kq} \sinh(kx_1) - \sinh(kx_0), & A_5 &= -\Gamma e^{-kq} \sinh(kx_1) - \sinh(kx_0), \end{aligned} \tag{4.4}$$

with

$$q = x_0 + d + x_1, \quad k = (1+\mathrm{i})/\sqrt{2} \tag{4.5}$$

A sample of the profiles of the basic flow and temperature are given in Figures 22 and 23.

The basic state fluxes can be shown to be

$$F_m = -\frac{1}{2} \mathrm{Im}\left\{ \frac{1}{k} \left[1 - e^{-2kx_0} - 4\Gamma \sinh(kx_0) e^{-kq} \sinh(kx_1) + \Gamma^2 \left(1 - e^{-2kx_1} \right) \right] \right\} \tag{4.6}$$

$$F_B = -\frac{1}{4} \mathrm{Im}\left(A_0 + \Gamma B_0 + \Gamma^2 C_0 \right) \tag{4.7}$$

where

$$\begin{aligned} A_0 &= x_0 e^{-2kx_0} + \frac{1}{2k}\left(1 - e^{-2kx_0}\right), \\ B_0 &= 2e^{-kq} \left\{ \left[-x_0 e^{-kx_0} + d \sinh(kx_0) \right] \sinh(kx_1) - \left[x_1 e^{-kx_1} + \frac{1}{k} \sinh(kx_1) \right] \sinh(kx_0) \right\}, \\ C_0 &= x_1 e^{-2kx_1} + \frac{1}{2k}\left(1 - e^{-2kx_1}\right), \end{aligned} \tag{4.8}$$

and

$$F_H = F_B - F_m \tag{4.9}$$

The fluxes here depend on four parameters x_0, x_1, d, Γ. They have a complicated dependence on these parameters. A sample is given in figures 24-26.

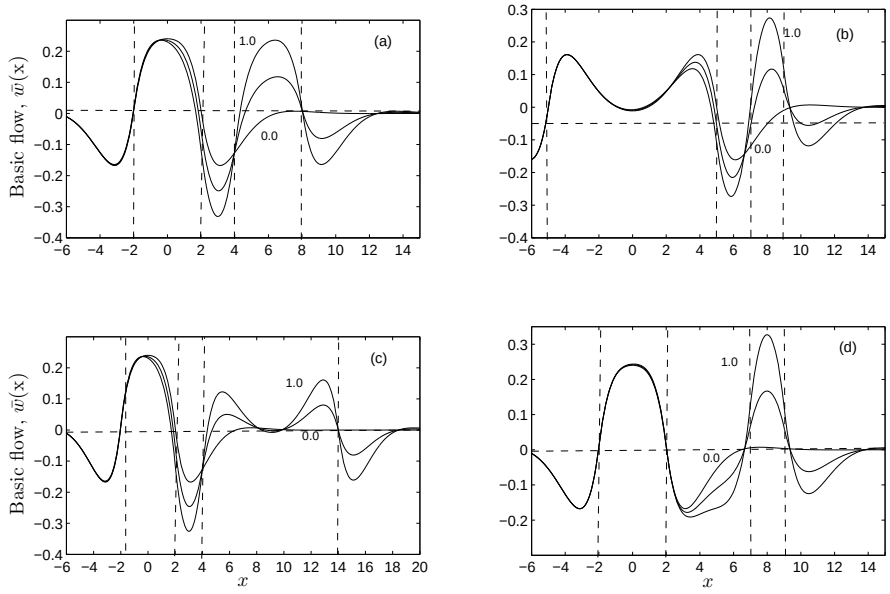

Figure 22. The profiles of the vertical basic flow, $\bar{w}(x)$, for some representative values of x_0, x_1, d, Γ. The labels refer to the value of Γ with the curve without label being for $\Gamma = 0.5$, while the figures (a), (b), (c), (d) correspond to (x_0, d, x_1) taking the sets of values (2.0,2.0,2.0), (5.0,2.0,1.0), (2.0, 2.0, 5.0), (2.0,5.0,1.0), respectively. Note that the curves for Γ =0.0 correspond to the solution of the single plume, and that when the plume is wide the flow can reverse within the plume, as in (c).

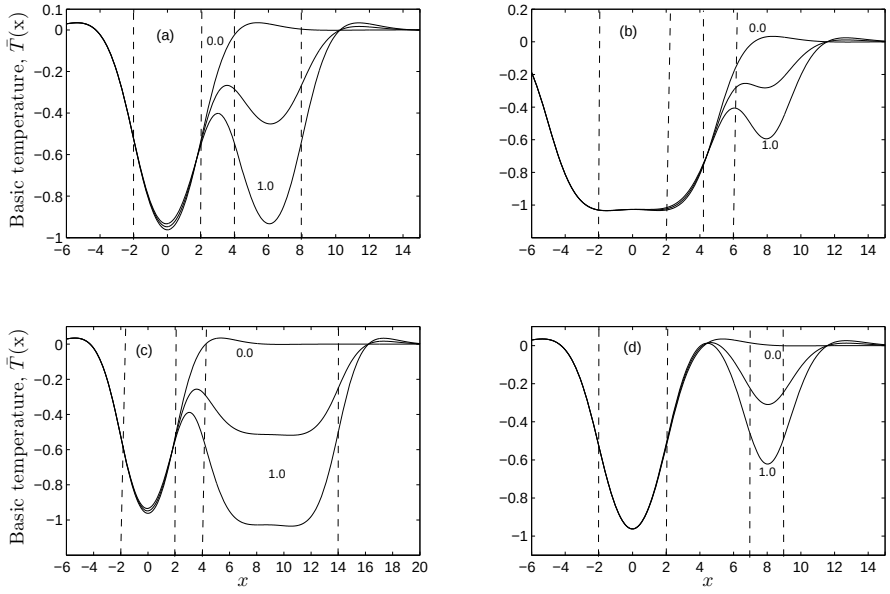

Figure 23. The profiles of the basic temperature, $\bar{T}(x)$, for representative values of x_0, x_1, d, Γ. The labels refer to the value of Γ with the curve without label being for $\Gamma = 0.5$ while the figures (a), (b), (c), (d) correspond to (x_0, d, x_1) taking the sets of values (2.0,2.0,2.0), (2.0,2.0,1.0), (2.0, 2.0, 5.0), (2.0,5.0,1.0), respectively.

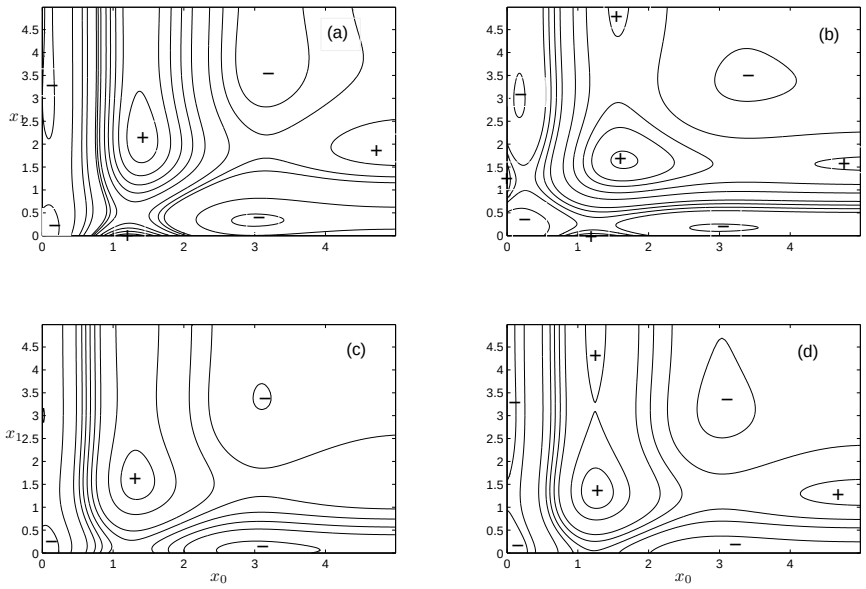

Figure 24. The buoyancy flux, F_B , of the two plume model in the (x_0, x_1) plane for (d, Γ) taking the values: (a) (1.0,0.5); (b) (1.0,1.0); (c) (2.0,0.5); (d) (3.0,0.5). Here + sign refers to a local maximum and - sign corresponds to a local minimum. . The overall maximum values of F_B in the form $\left(x_0, x_1, F_B\right)$ take the values: (a) (1.39,2.21,0.13293) (b) (1.66,1.66,0.19648); (c) (1.32,1.65,0.17658); (d) (1.25,1.44,0.18446). The overall minimum value is 0 at the origin for all cases.

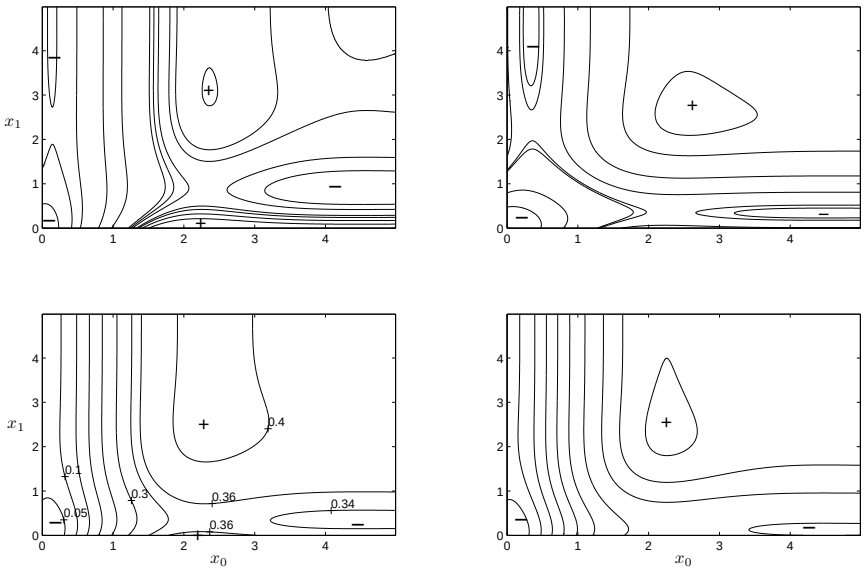

Figure 25. The material flux, F_m , for the same data as in Figure 5 above. The extremum values data in the form $\left(x_0, x_1, F_m\right)$ takes the values: (a) (2.22,0.0,0.36883); (b) (2.62,2.62,0.4743) (c) (2.37,2.53,0.4085); (d) (2.28,2.35,0.45362). The overall minimum value is 0 at the origin for all cases.

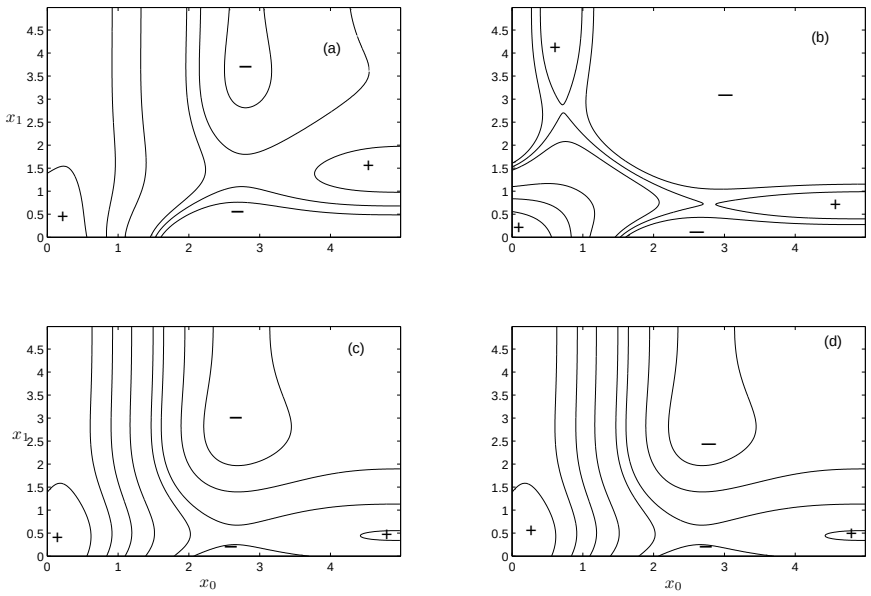

Figure 26.The heat flux, F_H, for the same data as in Figure 5 above. The overall minimum value, expressed in the form (x_0, x_1, F_H), takes the values: (a) (2.63, 0.0,-0.28277); (b) (3.12, 3.12,-0.3205); (c) (2.78, 3.01,-0.28245): (d) (2.61, 2.91,-0.32848).). The overall maximum value is 0 at the origin for all cases.

The stability problem here can be dealt with using the same method adopted for the single plume. The zeroth order problem has the solution

$$\left\{w_0^{(i)}, T_0^{(i)}, p_0^{(i)}, v_0^{(i)}\right\} = \sum_{j=1}^{3} \left\{\mu_j^3, \mu_j^2, \mu_j, -m\right\} A_j^{(i)} e^{-\lambda_j |x|}; \quad i = 4,5 \qquad (4.10)$$

$$\left\{w_0^{(i)}, T_0^{(i)}, p_0^{(i)}, v_0^{(i)}\right\} = \sum_{j=1}^{3} \left\{\mu_j^3, \mu_j^2, \mu_j, -m\right\} \left[A_j^{(i)} \cosh(\lambda_j x) + B_j^{(i)} \sinh(\lambda_j x)\right]; \; i = 1,2,3$$

(4.11)

$$u_0^{(4,5)} = \mp \sum_{j=1}^{3} A_j^{(4,5)} \lambda_j \exp\left(-\lambda_j |x|\right) \qquad (4.12)$$

$$u_0^{(i)} = \sum_{j=1}^{3} \lambda_j \left[A_j^{(i)} \sinh(\lambda_j x) + B_j^{(i)} \cosh(\lambda_j x)\right]; \quad i = 1,2,3 \qquad (4.13)$$

where the superscript 'i' refers to the region in as in Figure 21.

The application of the boundary conditions at the four interfaces $\pm x_0, c_1, d_1$ yields a quartic equation for the growth rate Ω_1 in place of (3.40) obtained for the single plume.

$$\left(\frac{\Omega_1}{in}\right)^4 + D_1\left(\frac{\Omega_1}{in}\right)^3 + D_2\left(\frac{\Omega_1}{in}\right)^2 + D_3\left(\frac{\Omega_1}{in}\right) + D_4 = 0 \qquad (4.14)$$

in which

$$D_1 = -\left(e_{00} + A_{11}\right), \quad D_2 = A_{12} + e_{00}A_{11} - a_{01}^2 + \Gamma\left(-a_{02}^2 + \Gamma a_{03}^2\right),$$
$$D_3 = -A_{13} - e_{00}A_{12} - a_{01}B_{11} + \Gamma\left(a_{02}B_{21} - a_{03}B_{31}\right), \tag{4.15}$$
$$D_4 = e_{00}A_{13} + a_{01}B_{12} + \Gamma\left(-a_{02}B_{22} + \Gamma a_{03}B_{32}\right).$$

$$A_{11} = e_{11} + e_{22} + e_{33},$$
$$A_{12} = e_{11}e_{22} + e_{11}e_{33} + e_{22}e_{33} - \Gamma a_{31}^2 + \Gamma a_{21}^2 - \Gamma^2 a_{23}^2, \tag{4.16}$$
$$A_{13} = e_{11}e_{22}e_{33} - \Gamma a_{31}^2 e_{22} + \Gamma a_{21}^2 e_{33} - \Gamma^2 a_{23}^2 e_{11},$$

$$B_{11} = -a_{01}\left(e_{22} + e_{33}\right) - \Gamma\left(a_{02}a_{21} + a_{03}a_{31}\right),$$
$$B_{12} = -a_{01}e_{22}e_{33} - \Gamma\left(a_{02}a_{21}e_{33} + a_{03}a_{31}e_{22}\right) \tag{4.17}$$
$$+ \Gamma^2\left(a_{01}a_{23}^2 - a_{02}a_{31}a_{23} - a_{03}a_{21}a_{23}\right),$$

$$B_{21} = -a_{01}a_{21} + a_{03}a_{23} + a_{02}\left(e_{11} + e_{33}\right), \tag{4.18}$$
$$B_{22} = -a_{01}a_{21}e_{33} + a_{03}e_{11}e_{33} + \Gamma\left(a_{01}a_{31}a_{23} - a_{03}a_{31}a_{21} + a_{03}a_{23}e_{11} - a_{02}a_{31}^2\right),$$
$$B_{31} = a_{01}a_{31} + a_{03}\left(e_{11} + e_{22}\right) + \Gamma a_{02}a_{23}, \tag{4.19}$$
$$B_{32} = a_{01}a_{31}e_{22} + a_{03}e_{11}e_{22} + \Gamma\left(-a_{01}a_{21}a_{23} + a_{02}a_{23}e_{11} + a_{02}a_{21}a_{31} + a_{03}a_{21}^2\right),$$

and

$$A_j^{(1)} = S_j\left[e^{-\lambda_j x_0} - \eta_1 e^{-\lambda_j x_0} - \eta_2\Gamma e^{-\lambda_j c_1} + \eta_3\Gamma e^{-\lambda_j d_1}\right] \tag{4.20}$$
$$B_j^{(1)} = S_j\left[e^{-\lambda_j x_0} + \eta_1 e^{-\lambda_j x_0} - \eta_2\Gamma e^{-\lambda_j c_1} + \eta_3\Gamma e^{-\lambda_j d_1}\right] \tag{4.21}$$
$$A_j^{(2)} = S_j\left[e^{\lambda_j x_0} - \eta_1 e^{-\lambda_j x_0} - \eta_2\Gamma e^{\lambda_j c_1} + \eta_3\Gamma e^{-\lambda_j d_1}\right] \tag{4.22}$$
$$B_j^{(2)} = S_j\left[-e^{\lambda_j x_0} + \eta_1 e^{-\lambda_j x_0} + \eta_2\Gamma e^{\lambda_j c_1} + \eta_3\Gamma e^{-\lambda_j d_1}\right] \tag{4.23}$$
$$A_j^{(3)} = S_j\left[e^{\lambda_j x_0} - \eta_1 e^{-\lambda_j x_0} - \eta_2\Gamma e^{-\lambda_j c_1} + \eta_3\Gamma e^{-\lambda_j d_1}\right] \tag{4.24}$$
$$B_j^{(3)} = S_j\left[-e^{\lambda_j x_0} + \eta_1 e^{-\lambda_j x_0} - \eta_2\Gamma e^{-\lambda_j c_1} + \eta_3\Gamma e^{-\lambda_j d_1}\right] \tag{4.25}$$
$$A_j^{(4)} = S_j\left[e^{\lambda_j x_0} - \eta_1 e^{-\lambda_j x_0} - \eta_2\Gamma e^{\lambda_j c_1} + \eta_3\Gamma e^{\lambda_j d_1}\right] \tag{4.26}$$
$$A_j^{(5)} = S_j\left[e^{-\lambda_j x_0} - \eta_1 e^{\lambda_j x_0} - \eta_2\Gamma e^{-\lambda_j c_1} + \eta_3\Gamma e^{-\lambda_j d_1}\right] \tag{4.27}$$

$$S_j = \frac{\mu_j^2}{2\lambda_j\left(2\mu_j + 3n^2\right)} \tag{4.28}$$

Here μ_j, λ_j are again given by (3.39). Using the properties of μ_j it can be shown that the all coefficients of (4.14) are real. Now the roots of any quadratic with real coefficients are either real or fall in pairs of complex conjugates. In general

$$\Omega_1 = in\,\mathrm{Re}\left\{\frac{\Omega_1}{in}\right\} - n\,\mathrm{Im}\left\{\frac{\Omega_1}{in}\right\} \tag{4.29}$$

Thus the roots of (4.14) are either all real in which case $\mathrm{Im}\left(\Omega_1 / \mathrm{i}n\right) = 0$ and Ω_1 is purely imaginary or there is at least a pair of complex conjugate roots for $\left(\Omega_1 / \mathrm{i}n\right)$. In

the former, the disturbance is neutral and the two plumes have a number of possible neutral modes that propagate with constant amplitudes. In the latter case, the imaginary parts of the complex root have different signs and Ω_1 as in (4.29) will have one root with positive imaginary and the other with positive real part. The root with the negative imaginary part gives an unstable mode whose amplitude grows like $\exp\left[-n\,\mathrm{Im}\left(\Omega_1 / \mathrm{i}n\right)\right]$. The condition for instability then is that equation (4.14) possesses complex roots.

The analysis shows that the quartic equation can always possess complex roots for some values of the wavenumber pair (m,n). Some of the results are illustrated in Figures 27 and 28.

The stability problem on the two plumes is then characterised by an increase in the order of magnitude of the growth rate for certain values of the parameters. The identification of those regions in the space of the parameters x_0, x_1, d, Γ is extremely complicated. Here we summarise the main results:

(i) When instability exists, as Γ increases from 0, the growth rate, Ω_c, of the preferred mode increases gradually reaching a maximum before it decreases to 0 at some value $\Gamma\left(x_0, x_1, d\right)$ which can be less than 1.0 in some cases.

(ii) For given x_0, x_1, Γ the growth rate, when instability exists, increases with d reaching a maximum before it decreases to 0 at some $d\left(x_0, x_1, \Gamma\right)$, and sometimes it appears again as d increased further but generally with a much smaller growth rate.

(iii) For given x_0, d, Γ the growth rate increases from 0 as x_1 increases from 0 reaching a maximum before it decreases to 0 and further increase of x_1 will see the appearance of instability again for large x_1. Instability can persist even if $x_1 \to \infty$.

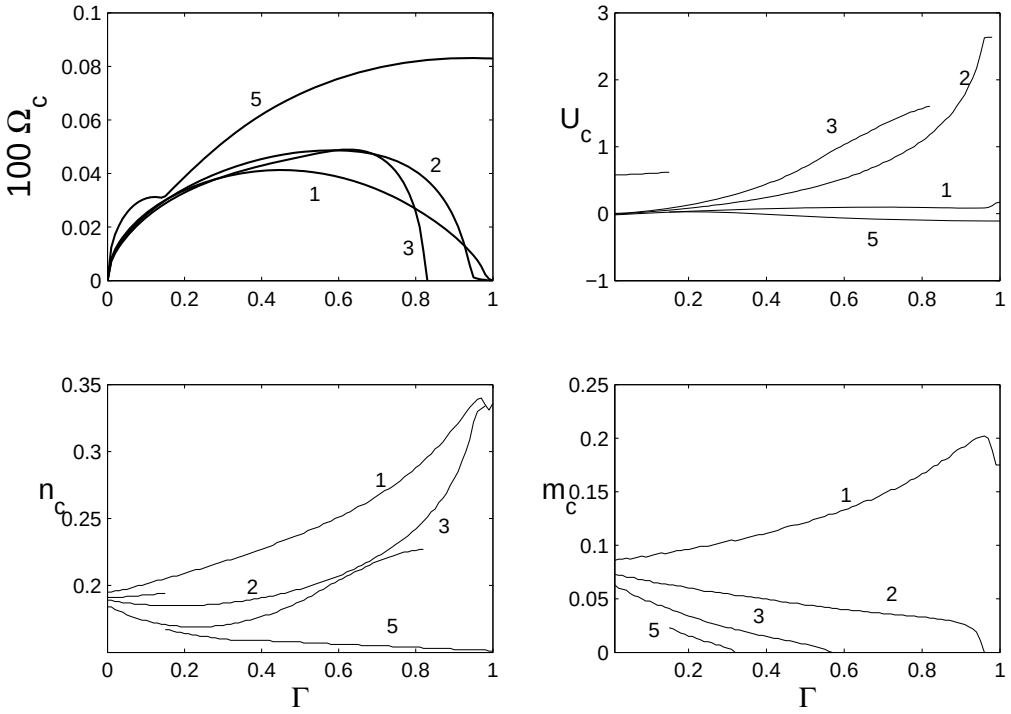

Figure 27. The preferred mode parameters as functions of Γ when $x_0 = 3.0, x_1 = 5.0$ for different values of d, as labelled. Note that the broken curve in U_z, n_c refers to the $d = 5.0$.

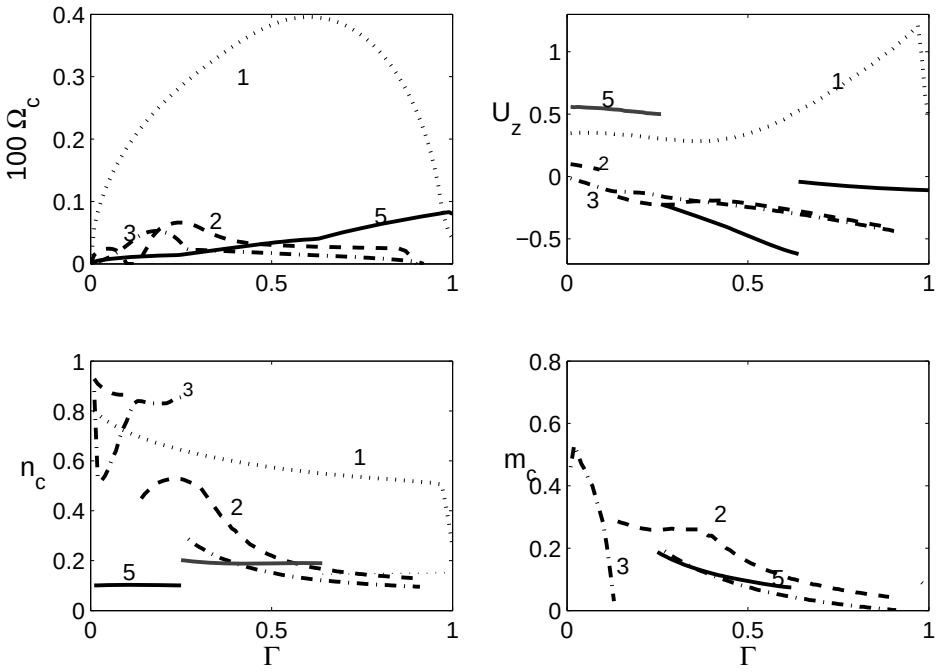

Figure 28. The preferred mode parameters as functions of Γ when $x_0 = 5.0, x_1 = 3.0$ for different values of d, as labelled. The dotted, broken, broken-dotted and solid curves refer to $d = 1, 2, 3, 5$, respectively.

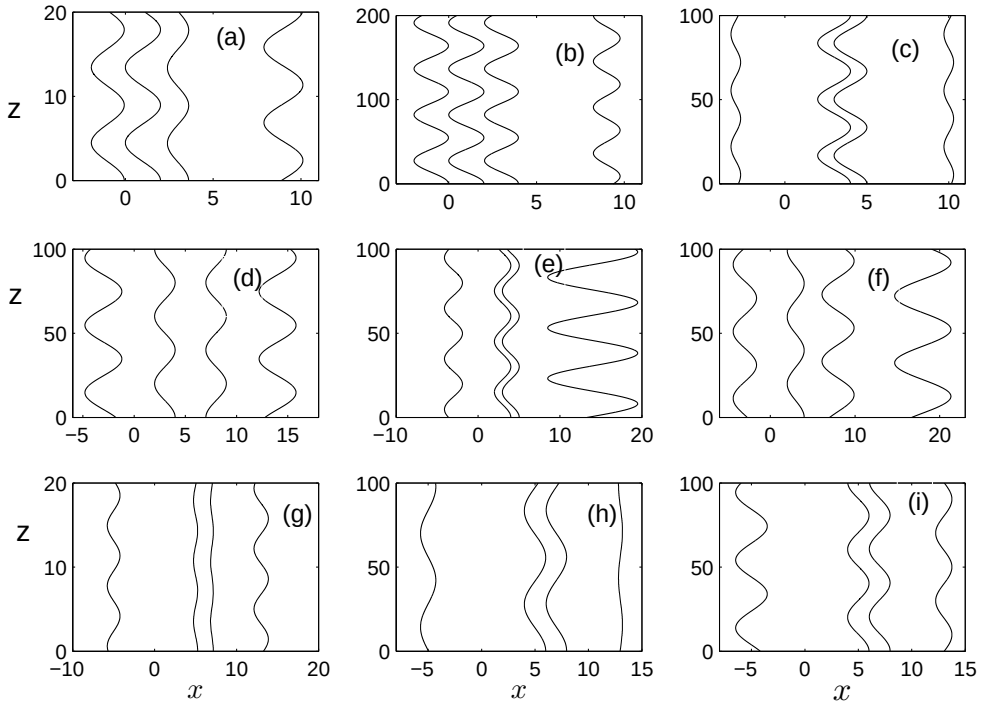

Figure 29. The types of profiles of the interfaces for the most unstable mode for some sample parameters (x_0, x_1, d, Γ). The data for the parameters for each sub-figure are shown in Table 1.

Energy considerations

The energy equations for the single interface derived in Eltayeb and Loper (1991) can be generalized to this case to get, in the present notation,

$$R\,\mathrm{Re}[\Omega][E_M + \sigma E_T] = -(D_M + D_T) + R\,\mathrm{Re}(M + \sigma H) + \mathrm{Re}(J) \quad (4.30)$$

$$R\,\mathrm{Im}[\Omega][E_M - \sigma E_T] = nR\,(E_{WT} - E_{WU}) + R\,\mathrm{Im}(M + \sigma H) + \mathrm{Im}(J) \quad (4.31)$$

where

$$E_M = \int_{-\infty}^{\infty} |\mathbf{u}|^2\,\mathrm{d}x \qquad D_M = \int_{-\infty}^{\infty} \left[\left| \frac{\mathrm{d}\mathbf{u}}{\mathrm{d}x} \right|^2 + (m^2 + n^2)|\mathbf{u}|^2 \right] \mathrm{d}x,$$

$$M = -\mathrm{i}\int_{-\infty}^{\infty} \frac{\mathrm{d}\bar{w}}{\mathrm{d}x} u w^*\,\mathrm{d}x, \quad E_{WU} = \int_{-\infty}^{\infty} \bar{w}\,|\mathbf{u}|^2\,\mathrm{d}x, \quad B = \int_{-\infty}^{\infty} w^* T\,\mathrm{d}x, \quad (4.32)$$

$$E_T = \int_{-\infty}^{\infty} |T|^2\,dx, \qquad D_T = \int_{-\infty}^{\infty} \left[\left| \frac{dT}{dx} \right|^2 + (m^2 + n^2)|T|^2 \right] dx,$$

$$H = -\mathrm{i}\int_{-\infty}^{\infty} \frac{d\bar{T}}{dx} u^* T\,dx, \qquad E_{WT} = \int_{-\infty}^{\infty} \bar{w}\,|T^2|\,dx, \quad (4.33)$$

$$J = w^*(-x_0)\left\langle \frac{\mathrm{d}w}{\mathrm{d}x} \right\rangle\Big|_{-x_0} + w^*(x_0)\left\langle \frac{\mathrm{d}w}{\mathrm{d}x} \right\rangle\Big|_{x_0} + w^*(c_1)\left\langle \frac{\mathrm{d}w}{\mathrm{d}x} \right\rangle\Big|_{c_1} + w^*(d_1)\left\langle \frac{\mathrm{d}w}{\mathrm{d}x} \right\rangle\Big|_{d_1} \quad (4.34)$$

where the jump $\langle\ \rangle$ is defined in (3.23) above.

When we substitute the expansion scheme defined by (3.24) into the two equations (4.30) and (4.31), and equate the coefficients of the different powers of R to zero, we obtain a hierarchy of systems of two coupled equations determining the growth rate and vertical phase speed at different orders of magnitude in R. The zeroth order equation from (4.30) represents a balance between the term $\left(D_{M0}+D_{T0}\right)$ representing the total (viscous and thermal) diffusion and the term $\mathrm{Re}\left(J_0\right)$ representing the transfer of compositional energy from the basic state through the variations of the basic state concentration, $\bar{C}$, of the light material. This balance does not involve the growth rate directly. It shows that the compositional buoyancy is the primary force balancing diffusion. The next order balance gives

$$\mathrm{Re}\left[\Omega\right]\left[E_{M0}+\sigma E_{T0}\right]=-\left(D_{M1}+D_{T1}\right)+\mathrm{Re}\left[M_0+\sigma H_0\right] \qquad (4.35)$$

in which the subscript 1 in D_{M1}, D_{T1} refers to the second order terms (i.e. of order R) in an expansion of these terms in R. Note that there is no $\mathrm{O}\left(R\right)$ term for J in (4.34) since Dw_1 is continuous across the interfaces. This balance is between the term $R\,\mathrm{Re}\left[\Omega\right]\left(E_M+\sigma E_T\right)$ representing the rate of change of total (kinetic + potential) energy density on one hand and the excess of total transfer of energy (kinetic + thermal) from the basic state to the waves through the basic state velocity and temperature gradients over second order loss of energy due to diffusion. This is the same expression obtained for the single Cartesian plume. In the case of the single plume, the solution falls into two uncoupled categories of even and odd solutions in x. As a consequence, the zeroth order solution has the variables w_0, T_0, p_0, v_0 having one parity while u_0 has a different parity. The first order solution is associated with w_1, T_1, p_1, v_1 having the parity of u_0 and u_1 having the parity of w_0, T_0, p_0, v_0. Since both $\bar{w}, \bar{T}$ are even in x, all the integrals on the right-hand side of (4.35) vanish in the case of the single plume. For the two plumes, on the other hand, such a clear division of parity is absent particularly when the two plumes are not identical (also see figure 17 below). As a result the integrals on the right-hand side of (4.35) do not vanish and consequently a non-zero growth rate is obtained. Even when the two plumes have the same thickness and the same strength (i.e., $\Gamma=1.0$), the four interfaces can possess solutions which lack symmetry. For example two interfaces can take varicose mode

parity while the other two take sinuous mode parity (see figure 17 (a)). While either plume can possess symmetry or anti-symmetry individually, the two plumes taken together may not possess symmetry or anti-symmetry. It can then be concluded that the nature of the instability for the two plumes is the same as that of the single plume but the lack of parity in the solution is the cause of the change of order of magnitude of the growth rate.

The helicity

The local helicity function, $H(x)$, vanishes everywhere for two-dimensional modes (i.e. when $m = 0$). While the helicity of a single plume is an odd function of x and hence its integral over the whole range of x vanishes even when $m \neq 0$, this may no longer be applicable when the motions are three-dimensional in the presence of a second plume. However, it was found here that the instability is mostly two-dimensional (i.e. m =0) and only in small intervals of some cases is the instability 3-dimensional and consequently the total helicity is non-zero.

5. References

Bonneville, A. Dosso, L and Hildenbrand, A. 2006. Temporal evolution of geochemical variability of the South Pacific superplume activity. *Earth Planet. Sci. letts.* **244**;251-269.

Classen, S, Heimpel, M and Christensen, U., Blob instability in rotating compositional convection. *Geophy. Research Lett.*, **26(1),** 135-138.

Copley, S.M., Giamel, A. F., Johnson, S.M. and Hornbecker, M.F., 1970. The origin of freckles in unidirectionally solidified castings. *Metall. Trans.*, 1970, **1**, 2193-2204.

Duncan, R.A. and Richards, M.A. 1991. Hotspots, mantle plumes, flood basalts and true polar wander. *Rev. Geophys*. **29**; 31-50.

Elbashir, T.B.A., Al-Lawati, M.A. and Eltayeb, I.A. 2010. The dynamics of compositional plumes. *Submitted*.

Eltayeb, I.A., 1999. The stability of compositional plumes in a rotating magnetic fluid. *Phys. Earth Planet inter*., **110**, 1-19.

Eltayeb, I.A., 2006. The stability of a compositional plume rotating in the presence of a magnetic field. *Geophy. Astrophys. Fluid Dynam.*, **100**,429-455.

Eltayeb, I. A. and Hamza, E.A., 1998. Compositional convection in the presence of rotation *J. Fluid Mech.,* **354**, 277-299.

Eltayeb, I.A., Hamza, E.A, Jervase, J.A., Krishnan, E.A. and Loper, D.E., 2004. Compositional convection in the presence of a magnetic field. I. A single interface. *Proc. R. Soc. Lond.A,* **460**, 3505-3528.

Eltayeb, I.A., Hamza, E.A, Jervase, J.A., Krishnan, E.A. and Loper, D.E., 2005. Compositional convection in the presence of a magnetic field. II. A Cartesian plume. *Proc. R. Soc. Lond* A, **461**, 2605-2633.

Eltayeb, I.A. and Loper, D.E., 1991. On the stability of vertical double-diffusive interfaces. Part 1. A single interface. *J. Fluid Mech.,* **228,** 149-181.

Eltayeb, I.A. and Loper, D.E., 1994. On the stability of vertical double-diffusive interfaces. Part 2. Two parallel interfaces. *J. Fluid Mech.,* **267,** 251-271.

Eltayeb, I.A. and Loper, D.E., 1997. On the stability of vertical double-diffusive interfaces. Part 3. Cylindrical interface. *J. Fluid Mech.,* **353,** 45-66.

Hauri, E.H., Whitehead, J.A. and Hart, S.R. 1994. Fluid dynamics and geochemical aspects of entrainment in mantle plumes. *J. Geophys. Res*. **99(B12),** 24275-24300.Hills, R.N., Loper, D.E. and Roberts, P.H. 1983. A thermodynamically consistent model of a mushy layer. *Quart. J. Mech. Appl. Math*. **36**, 505-539.

Huppert, H.E., 1990.The fluid dynamics of solidification. *J. Fluid Mech.,* **212**, 209-240.

Larson, R. and Olson, P. 1991. Mantle plumes control magnetic reversal frequency. *Earth Planet. Sci. Letts.* **107**; 437-447.

Loper, D.E., 1978. The gravitationally powered dynamo. *Geophys. J. R. Astron. Soc*., **54**,389-404.

Loper, D.E. (Ed.), 1987. *Structure and Dynamics of Partially Solidified Systems*. Dordrecht: Matinus Nijhoff.

Loper, D.E. and McCartney, K. 1986. Mantle plumes and the periodicity of magnetic field reversals. *Geophys. Res. Letters*. **13**;1525-1528.

Loper, D.E. and Moffatt, H.K., 1993. Small scale hydromagnetic flow in the Earth's core: rise of a vertical buoyant plume. *Geophys. Astrophys. Fluid Dyn.,* **68**,177-202.

Loper, D.E. and Roberts, P.H. 1979. Are planetary dynamos driven by gravitational settling? *Phys. Earth. Planet. Inters.* **20**; 192-193.

Loper, D.E. and Roberts, P.H. 1981. A study of conditions at the inner core boundary of the Earth. *Phys. Earth. Planet. Inters.* **24**;302-307.

Loper, D.E. and Roberts, P.H., 1983. Compositional convection and the gravitationally powered dynamo. In *Stellar and planetary magnetism.* Edited by A. M. Soward, pp.297-327. London: Gordon and Breach.

Loper, D.E. and Stacey, F.D. 1983. The dynamical and thermal structure of deep mantle plumes. *Phys. Earth Planet. Intr*. **33**;304-317.

Malkus, W.R.V. and Proctor, M.R.E. 1975. The macrodynamics of the α -effect dynamos in rotating fluids. *J. Fluid Mech*. **67**; 417-443.

Moffatt, H.K. 1970. Turbulent dynamo action at low magnetic Reynolds number. J. *Fluid Mech*. **41**; 435-452.

Moffatt, H.K., 1989. Liquid metal MHD and the geodynamo. In *Liquid Metal Magnetohydrodynamics*. (Eds. J. Lielpeteris and R. Moreau, pp403-412, Kluwer Academic Publishers).

Moffatt, H.K. and Loper, D.E. 1994. The magnetstrophic rise of a buoyant parcel in the Earth's core. *Geophys. J. Int.* **117**;394-402.

Morgan, W.J. 1971. Convection plumes in the lower mantle. *Nature* **230**; 42-43.

Nolet, G, Allen, R. and Zhao, D. 2007 . Mantle plume tomography. *Chem. Geology* **241**, 148-163.

Ribe, N.M. and Christensen, U.R. 1994. Three-dimensional modelling of plume-lithosphere interaction. *J. Geophys. Res.* **99(B1);** 669-682.

Roberts, P.H and Loper, D.E., 1983. Towards a theory of the structure and evolution of a dendrite layer. In *Stellar and Planetary Magnetism* (Ed. A. M. Soward, pp329-349, London: Gordon and Breach.

Sleep, N.H. 1990. Hotspots and mantle plumes: some phenomenology. *J. Geophys. Res*. **95(B5);** 6715-6736.

Steinberger,B. 2000. Plumes in a convecting mantle: models and observations for individual hotspots. *J. Geophys. Res*. **105(B5);**11127-11152.

White, R.S. and McKenzie. 1995. Mantle plumes and flood basalts. *J. Geophys. Res*. **100(B9);**17543-17585.

Worster, M.G., 1992. Instabilities of liquid and mushy regions during solidification of alloys. *J. Fluid mech*., **237**, 649-669.

Zhao, D. 2004. Global tomographic images of mantle plumes and subducting slabs: insight into deep Earth dynamics. *Physics Earth Planet. Intr.* **146**;3-34.